

NOAA Technical Report NOS 70 NGS 5



# **SELENOCENTRIC GEODETTIC REFERENCE SYSTEM**

Rockville, Md.

February 1977

**U.S. DEPARTMENT OF COMMERCE**  
**National Oceanic and Atmospheric Administration**  
National Ocean Survey

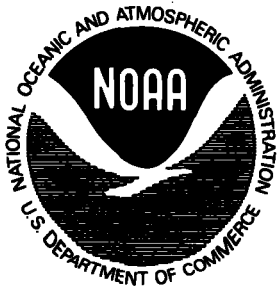
## NOAA TECHNICAL PUBLICATIONS

### National Ocean Survey-National Geodetic Survey Subseries

The National Geodetic Survey (NGS) of the National Ocean Survey establishes and maintains the basic National horizontal and vertical networks of geodetic control and provides Government-wide leadership in the improvement of geodetic surveying methods and instrumentation, coordinates operations to assure network development, and provides specifications and criteria for survey operations by Federal, State, and other agencies.

The NGS engages in research and development for the improvement of knowledge of the figure of the Earth and its gravity field, and has the responsibility to procure geodetic data from all sources, to process these data, and to make them generally available to users through a central data base.

NOAA Technical Reports and Memorandums of the NOS NGS subseries facilitate rapid distribution of material that may be published formally elsewhere at a later date. A listing of these papers appears at the end of this publication. This publication is available from the National Technical Information Service, U. S. Department of Commerce, Sills Building, 5285 Port Royal Road, Springfield, Va. 22151. Price on request.



NOAA Technical Report NOS 70 NGS 5

# SELENOCENTRIC GEODETTIC REFERENCE SYSTEM

Frederick J. Doyle  
Atef A. Elassal  
Topographic Division  
United States Geological Survey  
and

James R. Lucas  
Geodetic Research and Development Laboratory  
National Geodetic Survey

Rockville, Md.

February 1977

Originally prepared as Final Report  
under Contract T-1168B for the Lyndon  
B. Johnson Space Center, National  
Aeronautics and Space Administration,  
Houston, Texas.

## **U.S. DEPARTMENT OF COMMERCE**

**Juanita M. Kreps, Secretary**

## **National Oceanic and Atmospheric Administration**

Robert M. White, Administrator

## **National Ocean Survey**

Allen L. Powell, Director

## PREFACE

When the metric camera, stellar camera, laser altimeter package was implemented for the later Apollo missions it was evident that one of the major projects which could be performed was the establishment of a Selenocentric Control Network. Two members of the Apollo Orbital Science Photo Team, Frederick J. Doyle of the U.S. Geological Survey and Hellmut H. Schmid of the National Geodetic Survey, prepared essentially parallel proposals to perform this task. The analytical approach in each of the two proposals was nearly identical and it was obvious to the proposers that there would be little point in NASA undertaking both of them. By agreement within the Orbital Science Photo Team it was decided to submit a single proposal in response to memo change 36-NHB 80301A of February 1, 1971. Dr. Schmid would be the Principal Investigator with Mr. Doyle as Co-Investigator.

Contract T-1168B for experiment S-213 entitled Selenocentric Geodetic Reference System was awarded by NASA LBJ Space Center to the Geodetic Research and Development Laboratory of National Ocean Survey, and initial funding was provided in February of 1972.

Software development was begun immediately. Photographic mensuration was to be supplied by DMA/AC and DMA/TC, but this proceeded much more slowly than had been anticipated. Actual computations using real data were not begun until spring of 1974.

In January of 1974, Dr. Schmid went to Switzerland as a Visiting Professor at the Technical University in Zurich. Mr. Doyle took over the responsibilities of Principal Investigator. In September of 1974 Dr. Schmid retired from the National Geodetic Survey and moved permanently to Switzerland. By letter dated November 12, 1974, from Mr. Noel Hinners to the U.S. Geological Survey, Mr. Doyle was appointed Principal Investigator with Mr. James R. Lucas of National Geodetic Survey as Co-Investigator. Contract administration remained with National Geodetic Survey.

This document is the final technical report for contract T-1168B. Principal authors are Frederick J. Doyle, Atef A. Elassal, and James R. Lucas. The authors wish to acknowledge the technical contribution of the following individuals at National Geodetic Survey:

Robert Hanson	Chester Slama
Myron Lawrence	Allen Pope
Anna Mary Miller	

Mr. Bernard Chovitz was administrative officer at National Geodetic Survey and Mr. S. Nat Hardee, Jr. was the Contract Administrator at Johnson Space Center.

## Contents

		Page
	Preface .....	ii
	List of Tables .....	iv
	List of Figures .....	v
1.	Introduction .....	1
2.	Data Preprocessing .....	3
3.	Libration Model .....	5
4.	Mathematical Model for Lunar Orientation and Rotation .....	18
4.1	Relation between Inertial (XYZ) and Arbitrarily Oriented Rotating (X'Y'Z') Coordinate Systems .....	18
4.2	Photogrammetric Constraint for a Camera Photographing a Moving Object .....	20
4.3	Relationship between Differential Rotation Vector $\Delta \bar{T}_L$ and Differentials of Rotation Angles $(\alpha_t, \delta_t, \theta_t)$ .....	23
5.	Unified Least Squares System (ULSS) .....	23
6.	Photogrammetric Orientation of the Moon .....	27
6.1	The Apollo 15 Libration Solution .....	28
6.2	The Apollo 16 Libration Solution .....	33
6.3	Deviations of Moon's Photogrammetric Orientation from Eckhardt Libration Model .....	33
7.	Selenodetic Control Network .....	39
7.1	Bandwidth Minimization .....	39
7.2	Block Adjustment .....	41
7.3	Results of Block Adjustment .....	43
8.	Conclusions and Recommendations .....	49
8.1	Conclusions .....	49
8.2	Recommendations .....	50
	References .....	53

List of Tables

No.	Title	Page
1.	Libration in Node ( $\sigma$ ) .....	6
2.	Libration in Inclination ( $\rho$ ) .....	7
3.	Libration in Longitude ( $\tau$ ) .....	8
4.	Data Employed in Apollo 15 Libration Solution	29
5.	Data Employed in Apollo 16 Libration Solution	34
6.	Data Employed in Three Mission Libration Solution .....	38
7.	Components of Standard Deviation for Selected Exposure Stations .....	47
8.	Components of Standard Deviation for Simulated Test .....	48
9.	Systematic Differences in Map Graticule Resulting from Choice of Libration Model....	51

Mention of a commercial company or product does not constitute an endorsement by the NOAA National Ocean Survey. Use for publicity or advertising purposes of information from this publication concerning proprietary products or the tests of such products is not authorized.

## List of Figures

No.	Title	Page
1.	Libration in Node .....	10
2.	Libration in Inclination .....	11
3.	Libration in Longitude .....	12
4.	Right Ascension of Pole .....	13
5.	Declination of Pole .....	14
6.	Rotation Rate .....	15
7.	Fixed Inertial and Rotating Lunar Coordinate Systems .....	19
8.	Functional Chart of Unified Least Squares System ...	25
9.	Apollo 15 Computed North Pole Declination .....	30
10.	Apollo 15 Computed North Pole Right Ascension .....	31
11.	Apollo 15 Computed Angular Velocity .....	32
12.	Apollo 16 Computed North Pole Declination .....	35
13.	Apollo 16 Computed North Pole Right Ascension .....	36
14.	Apollo 16 Computed Angular Velocity .....	37
15.	Standard Deviation of Terrain Positions .....	45
16.	Spatial Distribution of Standard Deviations .....	46

## SELENOCENTRIC GEODETIC REFERENCE SYSTEM

Frederick J. Doyle

Atef A. Elassal

James R. Lucas

### 1. Introduction

After the successful landing on the Moon by Apollo 11, NASA chartered the Apollo Orbital Science Photo Team, with Frederick J. Doyle as chairman, to plan and supervise the acquisition of orbital science photography on the remaining missions. At that time the Apollo Program was planned for a total of twenty missions, and it was contemplated that several of these would be in high inclination orbits--perhaps even polar.

The Team immediately undertook development and implementation of a photogrammetric system which would provide accurate selenodetic positions and topographic mapping of all areas overflowed by the orbital spacecraft. The recommended system was operational by Apollo 15. In the meantime the program was reduced from twenty to seventeen missions, and the selection of landing sites reduced the total amount of coverage drastically below what had been anticipated.

The photogrammetric system was installed in the Scientific Instrument Module (SIM) bay of the Apollo Command Service Module (CSM). The system consisted of a 76-mm focal length mapping camera with  $74^\circ \times 74^\circ$  angular field, coupled with a stellar camera of 76-mm focal length and  $18^\circ \times 24^\circ$  angular field, and a laser altimeter with a  $300 \mu$  radian angular field and a least count of 1 meter. In addition, a panoramic camera with 610-mm focal length and  $11^\circ \times 108^\circ$  coverage was included to provide adequate resolution to support large-scale mapping.

In theory, this system provided everything (focal length excepted) that a photogrammetrist could want: The position of each exposure station would be obtained from Earth-based tracking; the orientation of each photograph could be computed from the synchronized stellar exposure and the lock-angles determined by preflight calibration; and the scale of each stereomodel would be obtained directly from the altimeter data.

Operationally, the data acquisition was adequate, but less than optimum. Orbital ephemerides provided by NASA were found to have large systematic deviations from the photogrammetrically determined spacecraft positions, at least for Apollo 15. For the other two



missions the deviations were smaller, but far from insignificant. These systematic errors are believed to be the result of the primitive orbit determination procedures in use at the time of the Apollo 15 mission, inadequate models of the lunar gravity field, and spacecraft oscillations induced by uncoupled thrusting and various activities of the astronauts.

The stellar camera, which was aimed near the pole of the orbit, was expected to provide mapping camera roll and yaw good to 5 arc seconds and pitch to 15 arc seconds. The larger pitch error is a consequence of the angular field of view of the stellar camera, which limits the precision of stellar camera yaw, and this angle corresponds to mapping camera pitch. Most of the stellar derived orientations were at or near the expected precision, but approximately 15 percent had errors several times this magnitude due to the small number and poor distribution of stars of sufficient brightness to be imaged by the stellar camera.

Furthermore, the laser altimeter failed early in the data collection phase of mission 15 and did not always function properly during the later missions. Consequently, range data were available for much less than half of the usable exposures.

The original objectives of the research effort were:

- (a) Provide a single integrated selenocentric control network with geodetic positions and elevations for numerous points within the area photographed
- (b) Provide a complete error analysis of the control network
- (c) Provide an independent solution of lunar physical libration parameters for the time of each mission
- (d) Provide a unified set of spacecraft positions as an aid to eventual refinement of the lunar gravity field
- (e) Derive a mathematical ellipsoidal figure for the Moon.

As the limitations in coverage and data quality developed, it became apparent that less than optimum results could be obtained. Particularly damaging was the failure to close the band of photography completely around the Moon. Nearly as bad was the limitation in latitude resulting from the selection of landing sites. These necessitated dropping objective (e) entirely, and greatly degraded the quality of results for objectives (a), (c), and (d).

An independent triangulation of the Apollo photographs was performed by the Defense Mapping Agency (DMA) to establish control for the mapping which was their primary responsibility. There are four significant differences between the DMA solution and that performed by NOS/USGS:

- (a) DMA used the orbital constraints provided by the tracking data to force a best fit between tracking and photogrammetry, while NOS/GS elected to abandon all tracking data for a purely photogrammetric solution.
- (b) DMA transformed the camera orientations from the inertial reference frame into the selenocentric coordinate system of date using the Koziel model for lunar librations, while NOS/GS used a model developed more recently by Eckhardt (1973).
- (c) DMA first reduced mission 15 and then fit 16 and 17 to these results, while NOS/GS performed a simultaneous adjustment of all three missions.
- (d) The computer program used by DMA did not include a covariance propagation capability.

Item (a) amounts to a fundamental difference in approach. Item (b) is explained in a subsequent section of this report. Items (c) and (d) are both related to the same operational problem: the simultaneous solution for 23,436 unknown parameters with complete covariance propagation requires a tremendous amount of "computer muscle," a program that can be tailored to the specific problem, the latest adjustment techniques, and a bit of luck.

## 2. Data Preprocessing

Selection, identification, and measurement of the terrain imagery were accomplished by the Defense Mapping Agency (DMA), which also performed the stellar mensuration and computed the camera orientation angles. Terrain image measurements and computed orientations were then supplied to the National Ocean Survey and the Geological Survey by DMA.

These data consisted of 12 passes (726 photos) from mission 15 and 8 passes (327 photos) from mission 17 which, together, covered a swath of varying width. The left hand limits are  $32^{\circ}$  N latitude,  $295^{\circ}$  longitude (measured eastward from the prime meridian); the right hand limits are  $24^{\circ}$  S latitude,  $205^{\circ}$  longitude. Along the equator, coverage is from  $35^{\circ}$  to  $140^{\circ}$  longitude. This swath is crossed at about  $70^{\circ}$  longitude by four passes (191 photos) from mission 16, which extended from  $12^{\circ}$  S latitude,  $330^{\circ}$  longitude to  $12^{\circ}$  N latitude,  $155^{\circ}$  longitude.

An inordinate portion of the manpower expended on this project was devoted to the preprocessing of these data, due primarily to the inability of the NOS computer to read any magnetic tape written by the DMA computers. A tape containing the mission 15 data could not be read on the first attempt because of parity error in a single record in the body of the data. A program was devised to skip records that were damaged by parity errors. On the second reading, more than 100 apparent parity errors were encountered, some of which had not been detected on the first reading. It appeared that these were caused by weak recorded signals that were below the threshold of the NOS reader heads, and that the recorded data were deteriorating with each reading. To make matters worse, through a misunderstanding, the data extracted from the tape on the second reading were destroyed before they could be copied to an NOS tape. The theory of continuing data deterioration was verified when, on the third and final reading, 600 records were lost to parity errors. These were finally recovered by key punching from hard copy supplied by DMA.

The data from mission 16 were supplied on cards, and the mission 17 data tape was read with only a few parity errors. However, shortly after the mission 16 data were reformatted and set up for use, DMA discovered a calibration error which invalidated these data and, subsequently, supplied a new set. Unfortunately, the new mission 16 data were completely unedited. A large number of misidentified images, causing residuals ranging from hundreds of microns to hundreds of millimeters, severely limited the size of data samples that could be handled in editing adjustments.

Furthermore, the mass of image data that had been measured by DMA, in order to insure a sufficient density of terrain points, served to increase the running time of all programs to a prohibitive level without contributing significantly to the quality of the results. Therefore, a program was devised to identify those terrain points whose images occurred in geometrically desirable areas on at least one photograph, i.e., within 5 millimeters of one of the 9 cardinal points. By discarding all terrain points that did not meet this criterion, the data set was reduced to manageable proportions without compromising the geometry. In fact, some frames contained more than 60 images of selected terrain points.

Fortunately, the orientation data supplied by DMA were in the Mean Celestial Coordinate System and had to be transformed into the True Selenocentric System of date. This facilitated the change of libration models, from Koziel to Eckhardt, which was found to be desirable after the preprocessing was nearly complete.

Just when it appeared that all data from all missions were correct and in the proper form, a number of ambiguities were discovered. Some of the numbers assigned to frames from mission 15 were duplicated on mission 17, and to make matters worse, the terrain points associated with laser range observations were assigned the same number as the exposure station with which they coincided. Apparently the adjustment programs used by DMAAC were capable of recognizing two or more separate entities with the same identifying number, but the MUSAT Program used by NOS/GS was not. Therefore, the exposure numbers of mission 17 had to be modified (these were changed back to their original designation for reporting their positions in Appendix B of this report), and some of the ground point numbers had to be modified. While this was not a large task, it required a large number of cards to be punched by hand, and extended the preprocessing time by several weeks.

### 3. Libration Model

Reduction of the stellar frames provides the orientation of each terrain exposure in the mean celestial coordinate system of 1950.0. The photogrammetric adjustments, on the other hand, must be performed in the true selenographic coordinate system of date. Transformation between these two coordinate systems requires a mathematical model of the lunar librations: the periodic variations in the orientation of the Moon's pole and fluctuations in its rate of rotation.

At the time when DMA began reducing Mission 15, available models of lunar librations were derived primarily from Earth-based optical observations. After consideration of models by Hayn, Koziel, and Eckhardt, DMA found that the differences among them were insignificant for the Apollo reduction and chose the Koziel model. By the time NOS/GS had all of the Apollo data in hand, more sophisticated models had been developed, using lunar laser ranging data and improved estimates of the third and fourth harmonic of the lunar gravity field. Consultation with scientists working in this field led us to prefer an improved Eckhardt model, and Don Eckhardt of AFCRL provided a computer program to employ this model.

A term-by-term comparison of the Koziel and Eckhardt models is provided by the following three tables, in which:

- $\ell$  is the mean anomaly of the Moon,
- $\ell'$  is the mean anomaly of the Sun,
- F is the geocentric angular distance from the ascending node of the lunar orbit to the Moon, and
- D is the geocentric angular separation of the Sun and Moon.

Table 1  
Libration in Node ( $\sigma$ )

Eckhardt Model:

$$\sigma = \frac{1}{I} \sum_{n=1}^{116} S_n \sin(i\ell + j\ell' + kF + mD) + \sum_{n=1}^{116} C_n \cos(i\ell + j\ell' + kF + mD) - 8''.12 \sin\Omega + \dots$$

where

$$I = 1^{\circ}32'30''.05 \approx 5400''$$

Koziel Model

$$\sigma = \frac{1}{\sin I} \sum_{n=1}^{11} S_n \sin(i\ell + j\ell' + kF + mD)$$

where

$$I = 1^{\circ}32'20''.0$$

and

Eckhardt Model		Koziel Model		Argument				Period
$S_n$	$C_n$	$S_n$	$C_n$	i	j	k	m	(days)
-101''.53	-0''.09	-102''.8		1	0	0	0	27.55
0.32	76.42	0.0		0	0	1	0	27.21
-24.77	0.15	-28.2		1	0	-2	0	26.88
-10.10	-0.00	-11.1		0	0	2	0	13.61
-3.00	-0.00	-3.3		0	0	2	-2	173.41
2.47	-0.00	2.2		1	0	0	-2	31.81
0.00	1.37	0.0		1	0	1	0	13.69
-0.90	-0.00	0.0		2	0	0	0	13.78
-0.81	-0.00	-0.6		1	0	2	0	9.11
0.71	0.68	0.0		1	0	-1	0	2195.12
-0.19	-0.01	0.1		2	0	-2	0	1097.56
.	.			.	.	.	.	
.	.			.	.	.	.	
.	.			.	.	.	.	

Table 2

Libration in Inclination ( $\rho$ )

Eckhardt Model:

$$\rho = \sum_{n=1}^{100} S_n \sin(il + jl' + kF + mD) - \sum_{n=1}^{100} C_n \cos(il + jl' + kF + mD) + 8''.24 \cos\Omega - \dots$$

Koziel Model:

$$\rho = \sum_{n=1}^{11} C_n \cos(il + jl' + kF + mD)$$

where

Eckhardt Model		Koziel Model		Argument				Period
$S_n$	$C_n$	$S_n$	$C_n$	i	j	k	m	(days)
0''.09	-99''.23		-100''.8	1	0	0	0	27.55
-76.46	0.32		0.0	0	0	1	0	27.21
0.14	24.84		28.2	1	0	-2	0	26.88
0.00	-10.56		-11.1	0	0	2	0	13.61
0.00	-3.08		-3.3	0	0	2	-2	173.41
-0.00	-1.94		-2.2	1	0	0	-2	31.81
0.00	-0.73		-0.6	1	0	2	0	9.11
-0.16	-0.73		0.0	1	0	-1	0	2195.12
-0.70	0.00		0.0	1	0	1	0	13.69
-0.00	0.51		0.0	1	0	2	-2	23.78
-0.01	-0.03		-0.1	2	0	-2	0	1097.56
.	.			.	.	.	.	
.	.			.	.	.	.	
.	.			.	.	.	.	

Table 3  
Libration in Longitude ( $\tau$ )

Eckhardt Model:

$$\tau = \sum_{n=1}^{73} S_n \sin (i\ell + j\ell' + kF + mD) + \sum_{n=1}^{73} C_n \cos (i\ell + j\ell' + kF + mD)$$

$$-7''44 \sin\Omega + 14''27 \sin(193^\circ44 - 0.004t) + \dots + 254''267$$

Koziel Model:

$$\tau = \sum_{n=1}^{12} S_n \sin(i\ell + j\ell' + kF + mD) + 7''6 \sin\Omega$$

where

Eckhardt Model		Koziel Model				Period (days)			
$S_n$	$C_n$	$S_n$	$C_n$	$i$	$j$	$k$	$m$		
90''30	0''01	82''4		0	1	0	0	365.26	
19.10	0.67	-7.5		2	0	-2	0	1097.56	
-16.70	-0.01	-15.6		1	0	0	0	27.55	
9.88	0.03	9.0		2	0	0	-2	205.95	
1.44	-8.64	0.0		1	0	-1	0	2195.12	
4.10	-0.00	3.7		1	0	0	-2	31.81	
-3.44	-0.00	-3.2		1	0	0	-1	411.90	
1.64	0.00	1.7		0	0	2	-2	173.41	
-1.22	0.00	0.0		1	-1	0	-1	3225.81	
0.95	0.00	0.8		2	-1	0	-2	472.19	
-0.48	-0.00	-0.6		0	0	0	2	14.76	
-0.44	-0.00	-0.4		2	0	0	0	13.78	
.	.			.	.	.	.		
.	.			.	.	.	.		
.	.			.	.	.	.		

Comparison of the tables reveals that, while there are small differences in the coefficients of the two models, the only large differences are:

(a) In the series for  $I\sigma$  the Eckhardt model contains a term,  $76''42 \cos F$ , which has no counterpart in the Koziel model.

(b) In the series for  $\rho$  the Eckhardt model contains a term,  $76''46 \sin F$ , which is also missing from Koziel.

(c) In the series for  $\tau$  the Eckhardt model contains a constant term of  $254''27$  and a 250 day periodic term with an amplitude of  $14''27$  which do not appear in Koziel. Furthermore the coefficients of the triennial term differ between the two models by  $26''6$ .

The additional terms in  $I\sigma$  and  $\rho$  serve to increase the amplitudes of the monthly variation in these librations by about 60%, as shown in figures 1 and 2. These terms are the result of incorporating the third harmonic of the lunar gravitational field into the libration model. Figure 3 shows that there is a large difference in  $\tau$  computed from the two models resulting from the factors listed above. This longitude offset is approximately  $230''$ ,  $275''$  and  $290''$  at the times of Apollo 15, 16, and 17 respectively.

These libration parameters can be expressed as variations in the right ascension and declination of the pole of rotation and the rotation rate using

$$\alpha_p = \tan^{-1} \left[ \frac{\cos(\Omega + \sigma) \sin(I + \rho) \cos \epsilon - \cos(I + \rho) \sin \epsilon}{-\sin(\Omega + \sigma) \sin(I + \rho)} \right]$$

$$\delta_p = \sin^{-1} \left[ \cos(\Omega + \sigma) \sin(I + \rho) \sin \epsilon + \cos(I + \rho) \cos \epsilon \right]$$

and

$$\text{Rotation Rate} = 13^{\circ}.1764/\text{day} + \frac{d\tau}{dt}$$

where  $\Omega$  is the longitude of the descending node of the lunar orbit,  $I$  is the mean inclination of the lunar equator with respect to the ecliptic, and  $\epsilon$  is the obliquity of the ecliptic. The variations in these parameters are shown in figures 4, 5, and 6.



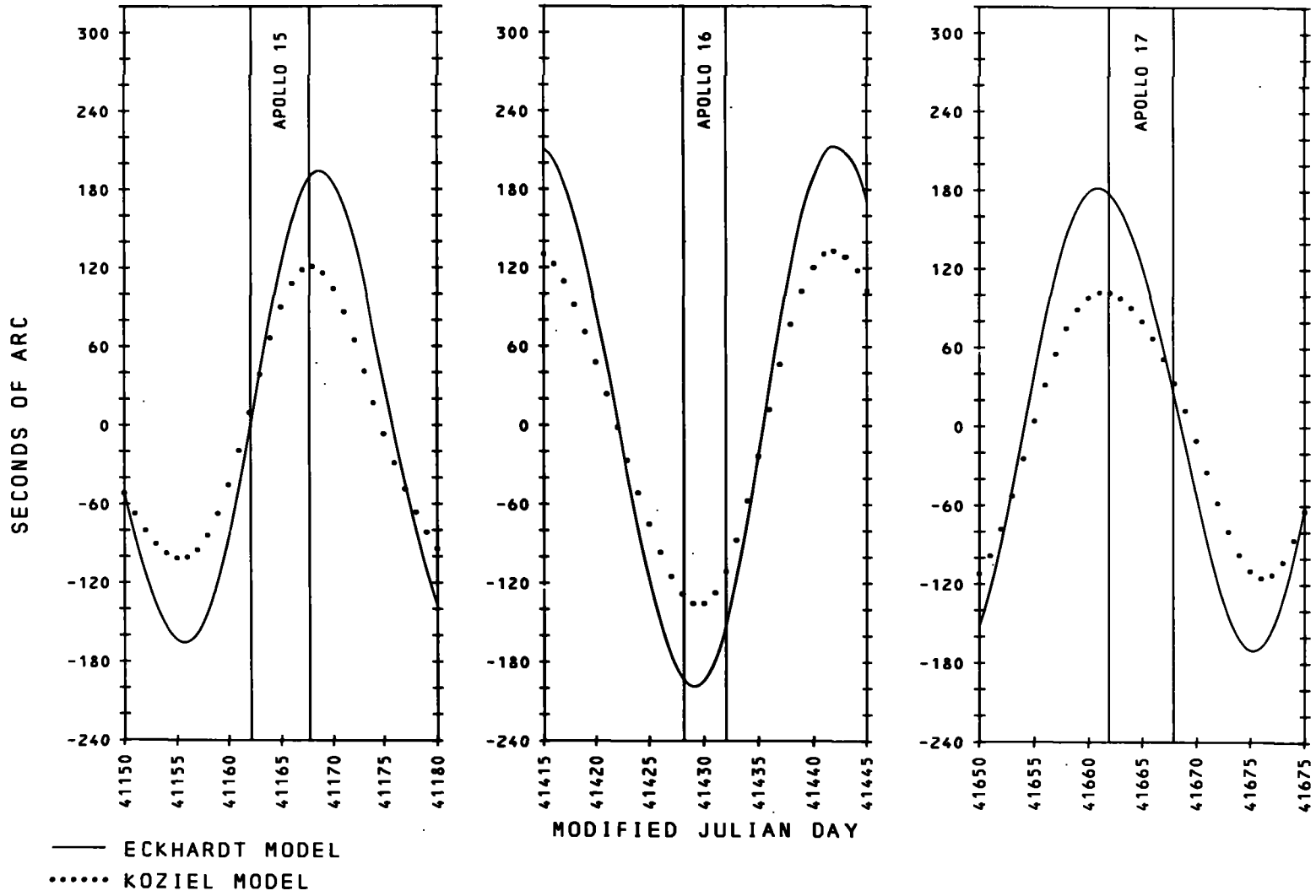


Figure 1.  
Libration in node.

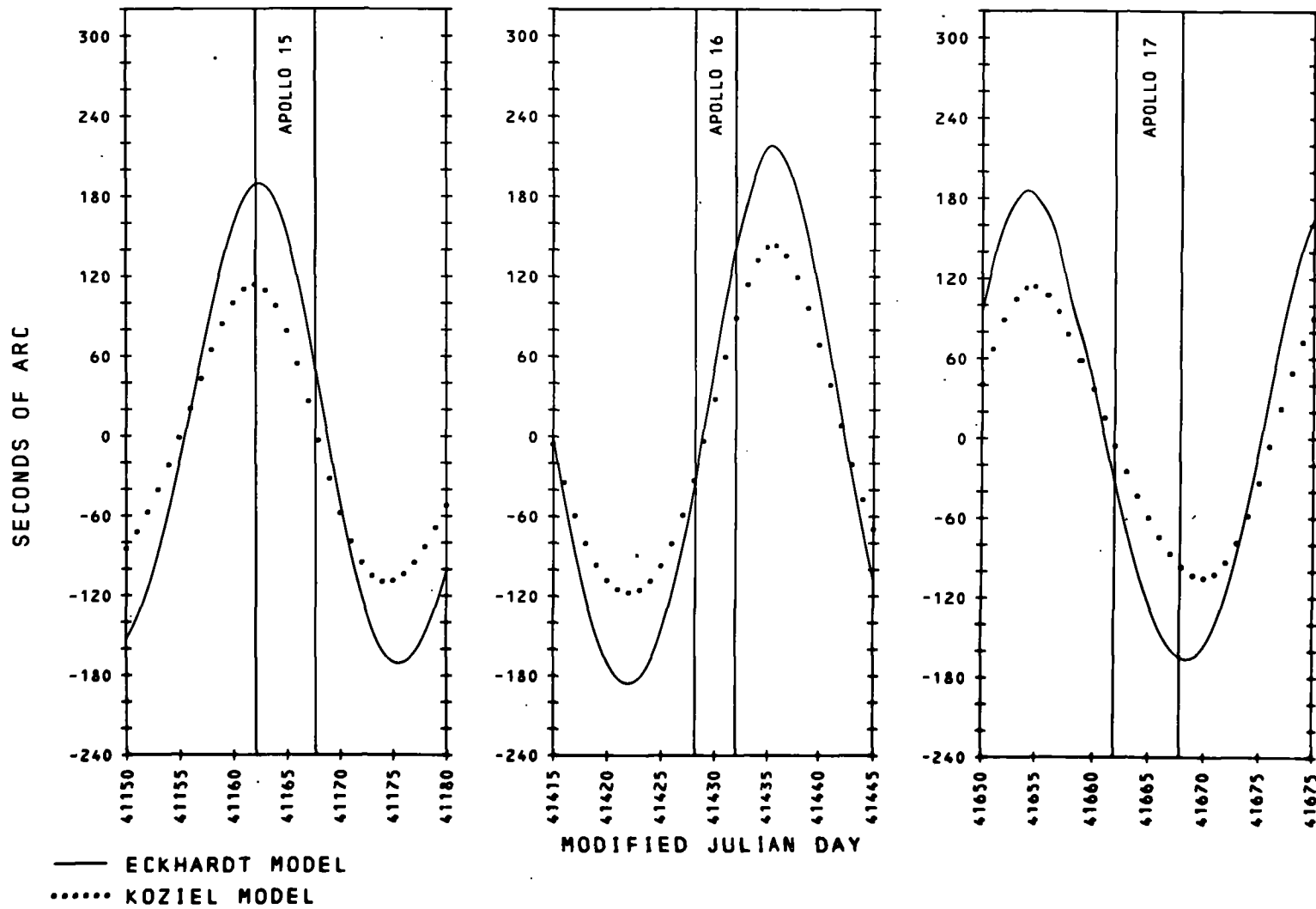


Figure 2.  
Libration in inclination.

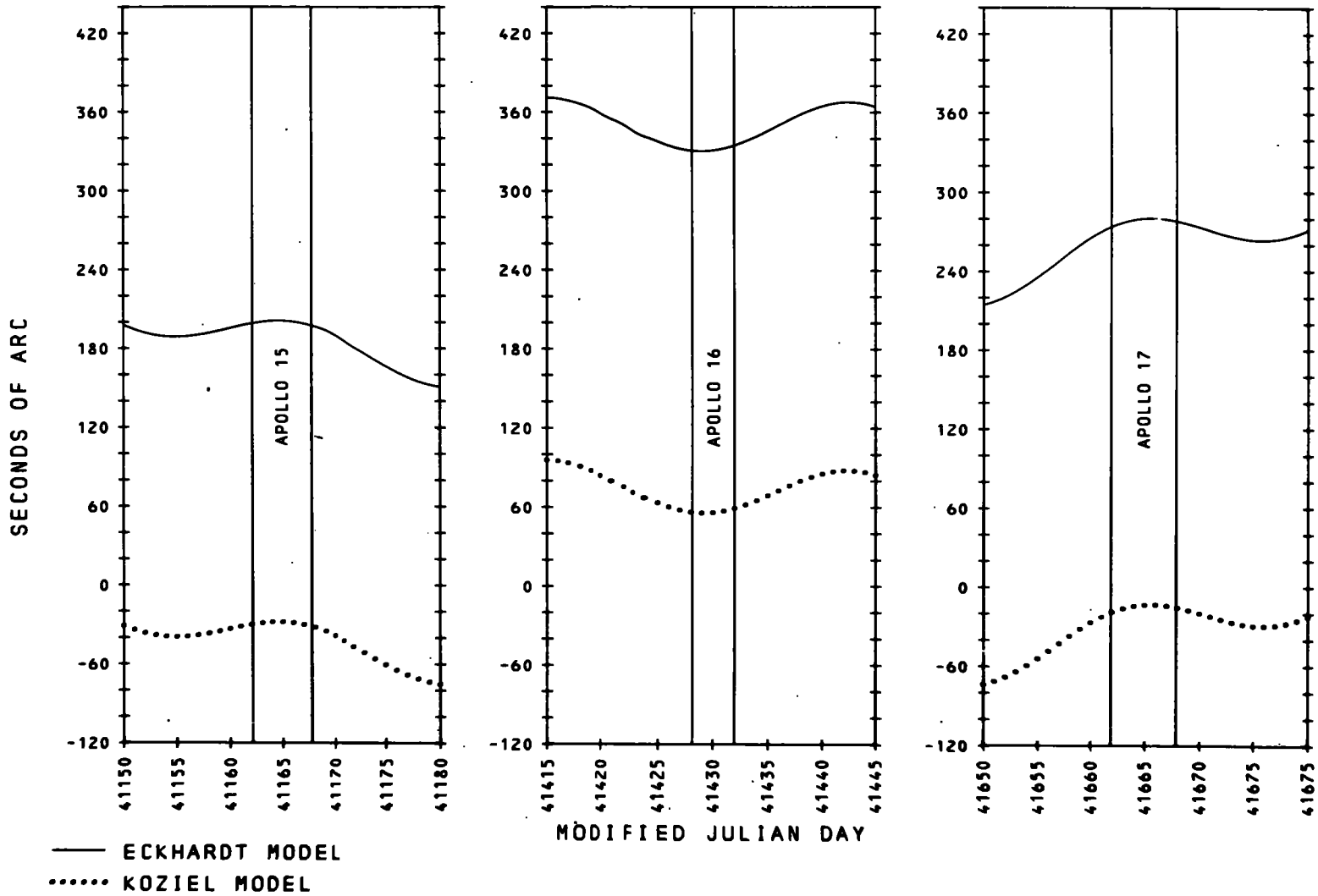


Figure 3.  
Libration in longitude.

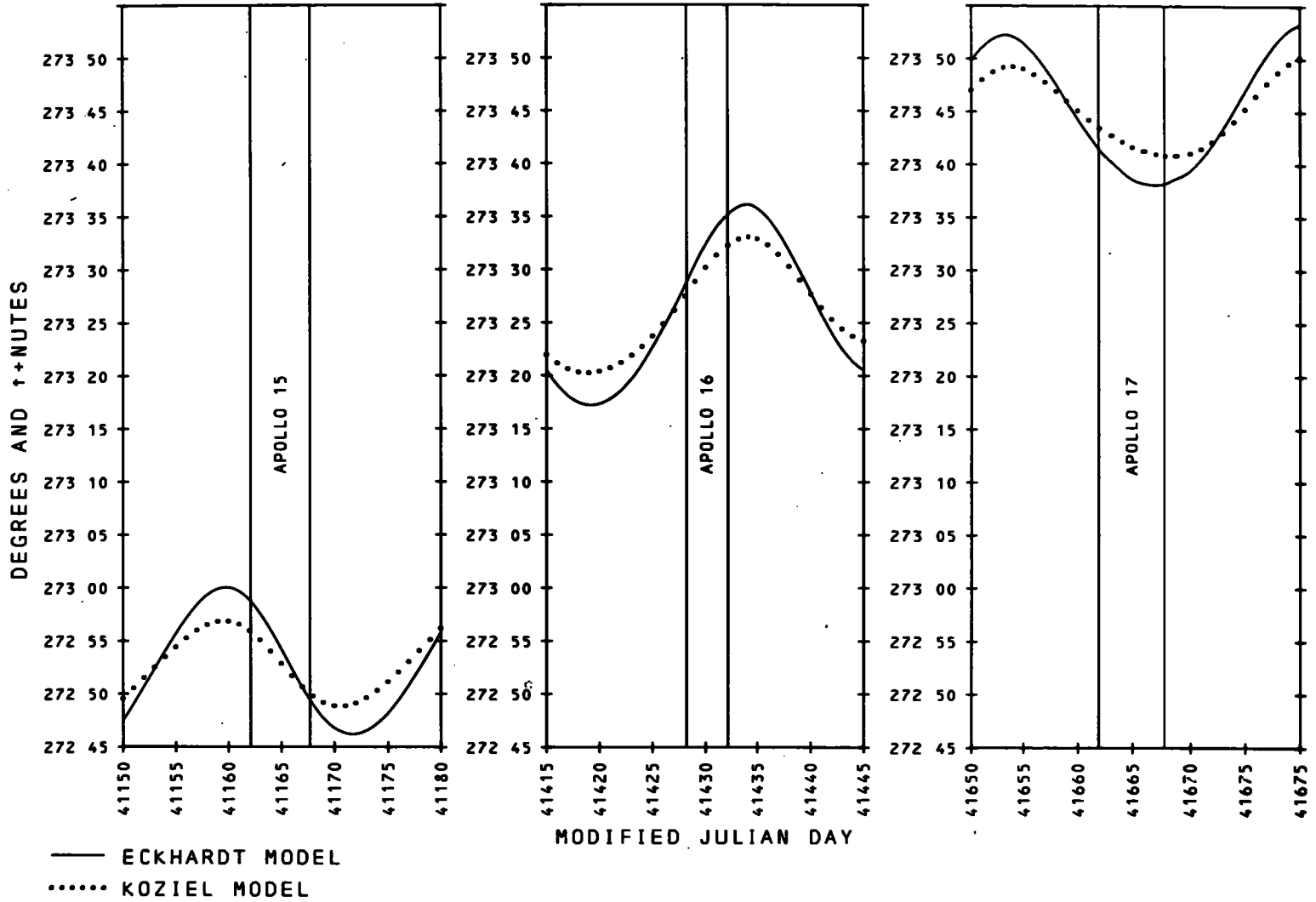


Figure 4.  
Right ascension of pole.

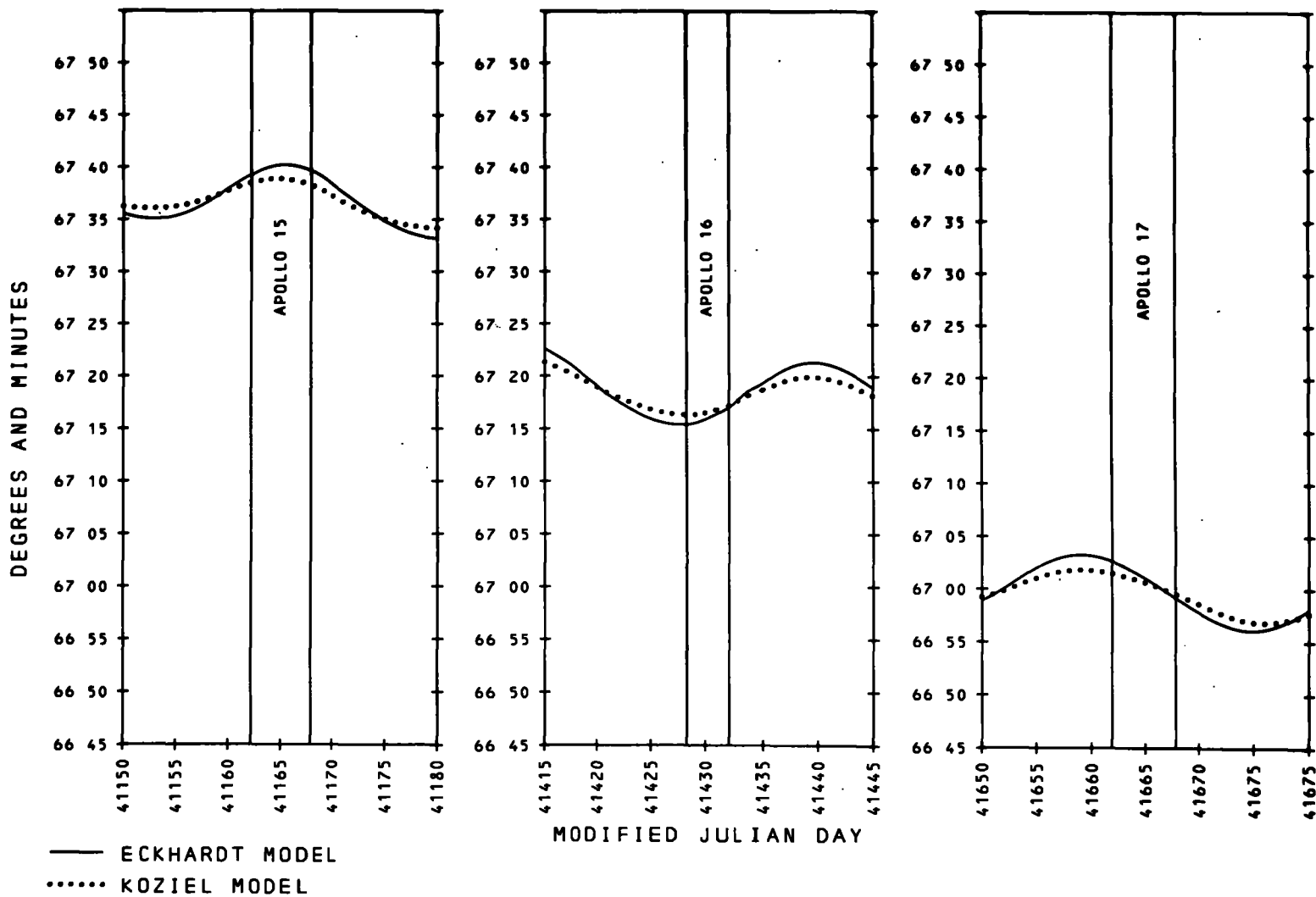


Figure 5.  
Declination of pole.

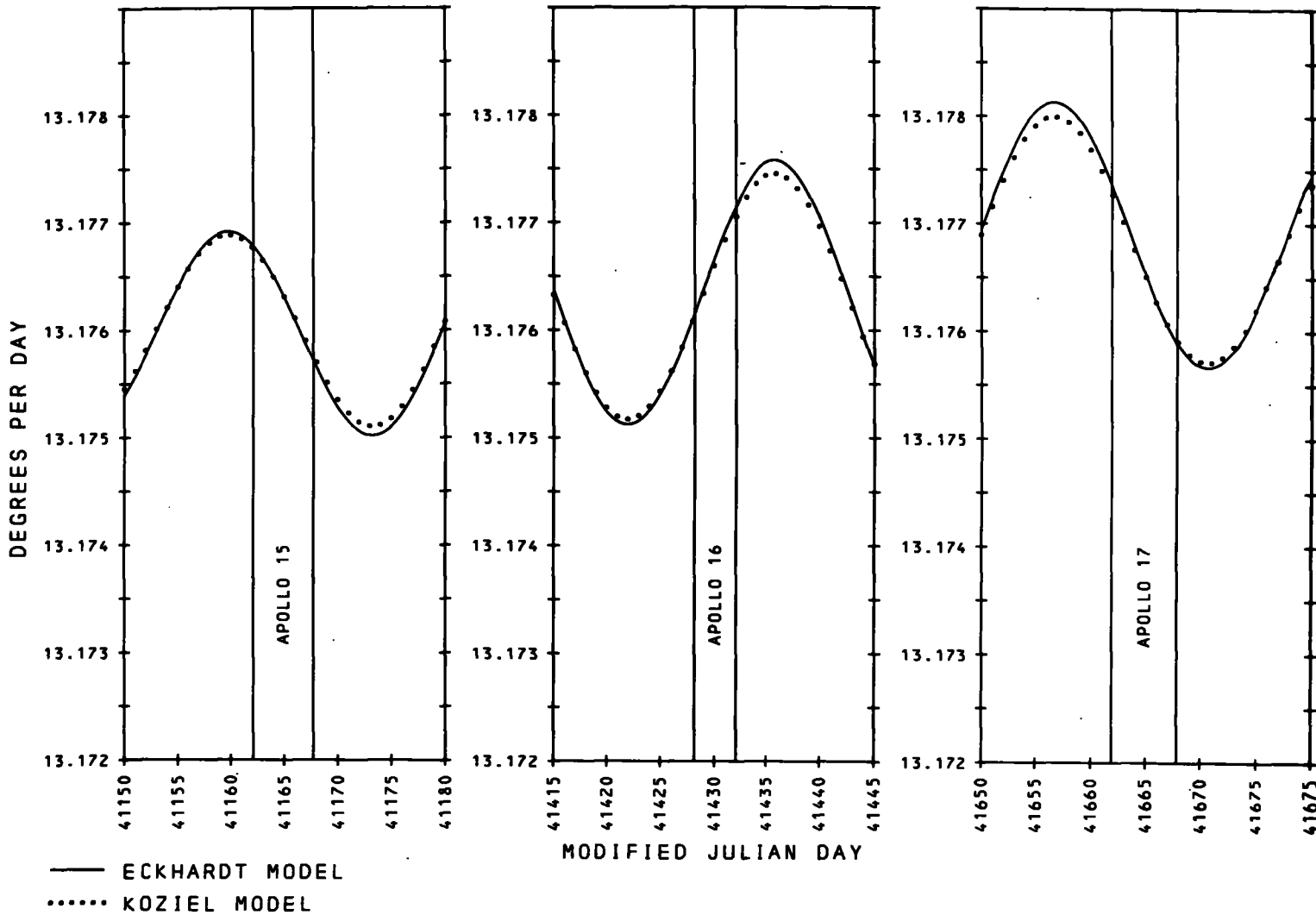


Figure 6.  
Rotation rate.

Since  $\sigma = (I\sigma)/I \approx 37(I\sigma)$  appears in the expressions for  $\alpha_p$  and  $\sigma_p$ , the variations in these quantities are considerably larger than those seen in  $I\sigma$  and  $\rho$ . However, the rotation rates computed from the two models agree to better than 0".5 per day which shows that there should be no problem in fitting the photographs into a single adjustment no matter which model is used.

On the other hand there is a significant difference between the Selenocentric coordinate systems defined by the two models. A point on the lunar surface (x,y,z) can be transformed into the ecliptic coordinate system using

$$\begin{bmatrix} x' \\ y' \\ z' \end{bmatrix} = R_3(\pi - \hat{\Omega}) R_1(-\hat{I}) R_3(-\hat{\theta}) \begin{bmatrix} x \\ y \\ z \end{bmatrix}$$

where

$$\hat{\Omega} = \Omega + \sigma$$

$$\hat{I} = I + \rho$$

$$\hat{\theta} = F - \sigma + \tau$$

and  $R_i$  is a rotation about the i-th axis through the argument. The inverse transformation will, of course, result in the original position (x, y, z). However, if the Eckhardt model is used to transform the position into the ecliptic system and the Koziel model is used for the inverse transformation, the result will be (x +  $\Delta x$ , y +  $\Delta y$ , z +  $\Delta z$ ).

Using differentials the following expressions can be derived

$$\Delta x = -y\Delta\hat{\theta} - z \sin\hat{\theta} \Delta\hat{I} + (z \sin\hat{I} \cos\hat{\theta} - y \cos\hat{I})\Delta\hat{\Omega}$$

$$\Delta y = x\Delta\hat{\theta} - z \cos\hat{\theta} \Delta\hat{I} - (z \sin\hat{I} \sin\hat{\theta} - x \cos\hat{I}) \Delta\hat{\Omega}$$

$$\Delta z = (x \sin\hat{\theta} + y \cos\hat{\theta}) \Delta\hat{I} - (x \sin\hat{I} \cos\hat{\theta} - y \sin\hat{I} \sin\hat{\theta})\Delta\hat{\Omega}$$

where

$$\Delta\hat{\Omega} = \sigma \text{ (Eckhardt)} - \sigma \text{ (Koziel)} \approx \frac{A}{I} \cos F$$

$$\Delta\hat{I} = \rho \text{ (Eckhardt)} - \rho \text{ (Koziel)} \approx A \sin F$$

$$\Delta\hat{\theta} = \tau \text{ (Eckhardt)} - \tau \text{ (Koziel)} - \Delta\hat{\Omega} \approx B - \frac{A}{I} \cos F$$

in which

$$A = 76'' \text{ expressed in radians}$$

and

$$B = 254'' - \text{long period terms (also in radians)}$$

Let the unit of length be the lunar radius and consider the point with  $\phi = 0$ ,  $\lambda = 0$ ,  $h = 0$  in the Selenocentric system defined by the Eckhardt model. In Koziel coordinates we have

$$x + \Delta x = 1$$

$$\begin{aligned} y + \Delta y &= \hat{\Delta\theta} + \hat{\Delta\Omega} \cos \hat{I} \\ &= B - \frac{A}{I} \cos F + \frac{A}{I} \cos F \cos \hat{I} \\ &\approx B \end{aligned}$$

$$\begin{aligned} z + \Delta z &= \hat{\Delta I} \sin \hat{\theta} - \hat{\Delta\Omega} \sin \hat{I} \cos \hat{\theta} \\ &= -A \sin F \sin \hat{\theta} - \frac{A}{I} \cos F \sin \hat{I} \cos \hat{\theta} \\ &\approx -A \sin F \sin \hat{\theta} - A \cos F \cos \hat{\theta} = -A \cos(F - \hat{\theta}) \\ &\approx -A \cos(\sigma - \tau) \end{aligned}$$

Since  $\sigma - \tau$  varies between plus and minus  $2^\circ$ ,  $z + \Delta z \approx -A$ , and

$$\Delta\phi \approx \sin^{-1}(-A) = 76''$$

$$\Delta\lambda \approx \tan^{-1}(B) = 254'' + \text{long period terms}$$

This shift of the Moon's principal axis was reported by Williams et al (1973). Following the same procedure for the point  $\phi = 0$ ,  $\lambda = 90^\circ$ ,  $h = 0$ , obtains

$$\Delta\phi \approx 0$$

$$\Delta\lambda \approx 254'' + \text{long period terms}$$

Hence the differences between the selenocentric coordinate systems defined by the two models are approximately:



(a) a rotation about the y-axis of 76"

(b) a rotation about the z-axis of 254" plus long period terms, resulting in 230" for Apollo 15, 275" for Apollo 16, and 290" for Apollo 17.

The longitude differences between missions would create a problem if the Koziel model were to be used and the tracking ephemeris rigidly enforced. DMA used the Koziel model, but did not hold to the ephemeris. In this block adjustment the ephemeris positions are not enforced and the Eckhardt model is used. Therefore, both adjustments are internally consistent, but since they are referred to slightly different selenocentric coordinate systems, there will be differences in the reported coordinates. These can amount to as much as 76" (640 meters) in latitude at  $\lambda = 0^\circ$  or  $180^\circ$  and 230" (1,938 meters) in longitude for points on the equator.

#### 4. Mathematical Model for Lunar Orientation and Rotation

Since stellar camera orientation is computed in the celestial inertial coordinate system, and this orientation is transferred to the lunar surface via the calibrated locking angles between the stellar and mapping cameras and the photogrammetric solution, it is possible to compute the orientation and rotation rate of the Moon (physical librations) purely from the photogrammetric data. This requires the formulation of a mathematical model between the fixed (celestial) and the rotating (lunar) coordinate systems.

##### 4.1 Relation between Inertial (XYZ) and Arbitrarily Oriented Rotating (X'Y'Z') Coordinate Systems

Assume (X,Y,Z) to be a rectangular inertial coordinate system and (X',Y',Z') to be a rectangular coordinate system rotating around its Z'-axis. Let the right ascension  $\alpha$  and declination  $\delta$  be the two angles defining the orientation of the axis of rotation Z' in the inertial system (X,Y,Z). Furthermore, let  $\theta$  be the rotation angle of (X',Y',Z') system around Z'-axis (Figure 7).

The rotation between (X,Y,Z) and (X',Y',Z') is given by the transformation matrix  $[L]$ , made up of three sequential rotations  $\alpha$ ,  $\delta$ , and  $\theta$ .

$$\begin{bmatrix} X \\ Y \\ Z \end{bmatrix} = [L] \begin{bmatrix} X' \\ Y' \\ Z' \end{bmatrix}$$

$z, z_1$        $z_2, z'$

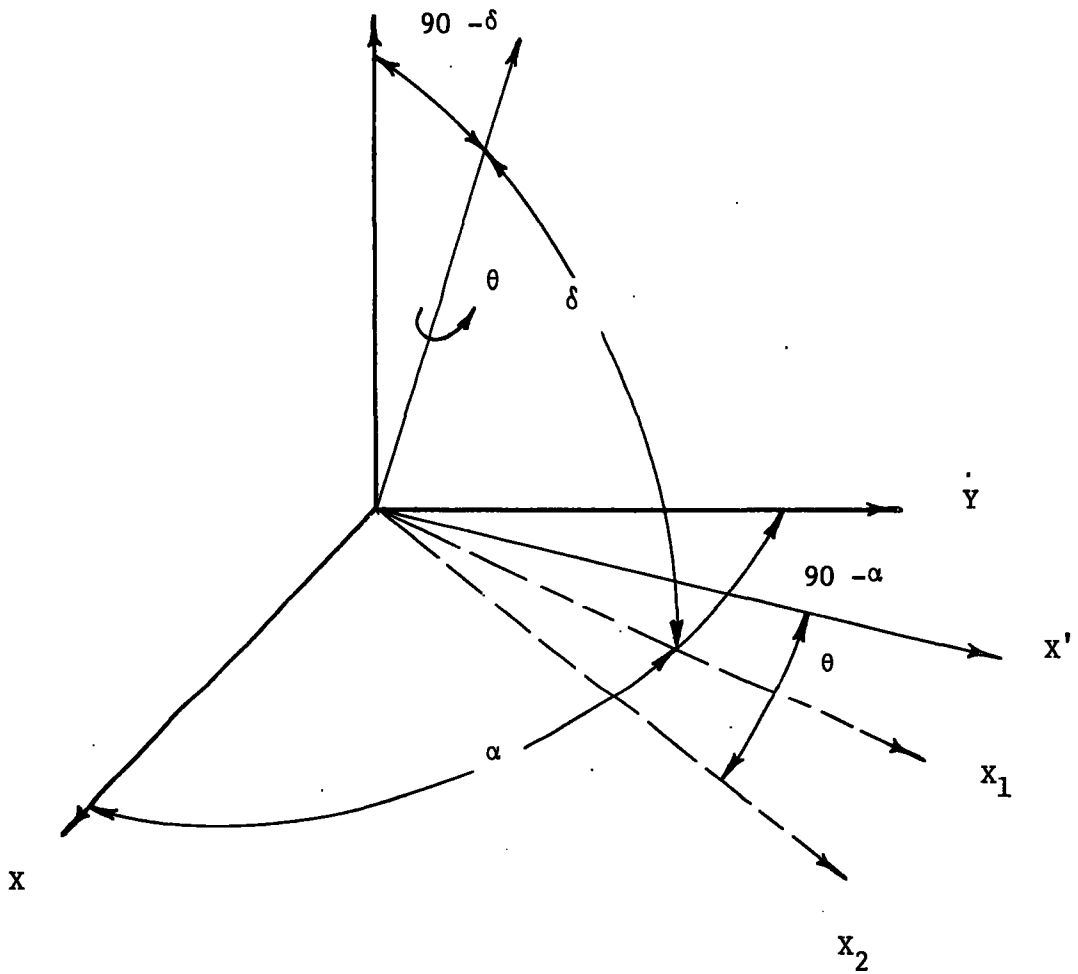


Figure 7.  
Fixed Inertial and Rotating Lunar Coordinate Systems

$$[L] \begin{bmatrix} \cos \alpha & -\sin \alpha & 0 \\ \sin \alpha & \cos \alpha & 0 \\ 0 & 0 & 1 \end{bmatrix} \begin{bmatrix} \sin \delta & 0 & \cos \delta \\ 0 & 1 & 0 \\ \cos \delta & 0 & \sin \delta \end{bmatrix} \begin{bmatrix} \cos \theta & -\sin \theta & 0 \\ \sin \theta & \cos \theta & 0 \\ 0 & 0 & 1 \end{bmatrix} \quad (4-1)$$

The three angles  $\alpha$ ,  $\delta$ , and  $\theta$  could be assumed to be time polynomials of the form:

$$\gamma_t \text{ (rotation)} = \sum_{i=0}^{i=n} K_{\gamma_i} (t)^i \quad \left\{ \gamma_t = \alpha_t, \delta_t, \theta_t \right\}$$

where,

$K_{\gamma_i}$  are unknown polynomial coefficients, and

$t$  is time from epoch  $t_0$ .

It is anticipated that in reducing Apollo data,  $\alpha$  and  $\delta$  rotations will be held constant for each mission and  $\theta$  will be a common first order time polynomial for all missions.

#### 4.2 Photogrammetric Constraint for a Camera Photographing a Moving Object.

The condition for the instantaneous collinearity of an object point, lens perspective center, and point image is expressed by the equation:

$$\begin{aligned} \vec{x} &= \begin{bmatrix} x_1 \\ x_2 \\ x_3 \end{bmatrix} = \gamma \begin{bmatrix} M \\ L \end{bmatrix} \begin{bmatrix} X_1^G - X_1^C \\ X_2^G - X_2^C \\ X_3^G - X_3^C \end{bmatrix} = \gamma \begin{bmatrix} M \\ L \end{bmatrix} \left\{ \vec{X}^G - \vec{X}^C \right\} \\ &= \gamma \begin{bmatrix} M \\ L \end{bmatrix} \vec{X} = \gamma \vec{X}' \end{aligned} \quad (4-2)$$

where:

- $\vec{x}$  is a vector of image space coordinates of image point.
- $\vec{X}^G$  is a vector of object space coordinates of object point.
- $\vec{X}^C$  is a vector of object space coordinates of lens center
- $\gamma$  a constant of proportionality
- [M] rotation matrix relating inertial and image reference systems
- [L] rotation matrix relating selenocentric and inertial reference systems.

Eliminating  $\gamma$  from equation (4-2) results in two condition equations which express the geometric requirements for collinearity of object, lens center, and image points.

$$\left. \begin{aligned} 0 = F_1 &= x_1 - x_3 \frac{X_1^I}{X_3^I} = x_1 - a x_3 \\ 0 = F_2 &= x_2 - x_3 \frac{X_2^I}{X_3^I} = x_2 - b x_3 \end{aligned} \right\} \quad (4-3)$$

Linear approximation of equation (4-3) can be obtained by employing a Taylor expansion, neglecting second and higher order terms:

$$\begin{bmatrix} \Delta F_1 \\ \Delta F_2 \end{bmatrix} = \begin{bmatrix} 1 & 0 & -a^0 \\ 0 & 1 & -b^0 \end{bmatrix} \begin{bmatrix} \Delta x_1 \\ \Delta x_2 \\ \Delta x_3 \end{bmatrix} - c^0 \begin{bmatrix} 1 & 0 & -a^0 \\ 0 & 1 & -b^0 \end{bmatrix} \begin{bmatrix} \Delta X_1^I \\ \Delta X_2^I \\ \Delta X_3^I \end{bmatrix} \quad (4-4)$$

where, superscript 0 denotes evaluation at the point around which Taylor expansion is computed. In order to maintain compact notation, the superscript 0 will be dropped in subsequent formulations.

In equation (4-4)

$$\Delta F_1 = a x_3 - x_1$$

$$\Delta F_2 = b x_3 - x_2$$

$$c = x_3 / X_3^I$$

Equation (4-4) in matrix notation is:

$$\vec{\Delta F} = [A] \vec{\Delta x} - c [A] \Delta X' \quad (4-5)$$

since,

$$\vec{X}' = [M] [L] \left\{ \vec{X}^G - \vec{X}^C \right\} = [M] [L] \vec{X}$$

then

$$\vec{\Delta X}' = [\Delta M] [L] \vec{X} + [M] [\Delta L] \vec{X} + [M] [L] \Delta \vec{X} \quad (4-6)$$

Applying the notion of differential rotation vector to equation (4-6), that is,

$$[\Delta M] = \left[ S_{\Delta \vec{T}_M} \right] [M] \quad (4-7)$$

in which  $\left[ S_{\Delta \vec{T}_M} \right]$  is a  $3 \times 3$  skew-symmetric matrix in the elements

$\left( \delta T_{M_1}, \delta T_{M_2}, \delta T_{M_3} \right)$  of the differential rotation vector  $\Delta \vec{T}_M$ .

Equation (4-6) can now be written as:

$$\begin{aligned} \vec{\Delta X}' &= \left[ S_{\Delta \vec{T}_M} \right] [M] [L] \vec{X} + [M] \left[ S_{\Delta \vec{T}_L} \right] [L] \vec{X} + [M] [L] \Delta \vec{X} \\ &= \left[ S_{\Delta \vec{T}_M} \right] \vec{X}' + [M] \left[ S_{\Delta \vec{T}_L} \right] \vec{X}'' + [M] [L] \Delta \vec{X} \\ &= - \left[ S_{\vec{X}'} \right] \Delta \vec{T}_M - [M] \left[ S_{\vec{X}''} \right] \Delta \vec{T}_L + [M] [L] \Delta \vec{X} \end{aligned} \quad (4-8)$$

Substituting (4-8) into (4-5) results in the condition equation

$$\begin{aligned} \vec{\Delta F} &= [A] \Delta \vec{x} + c [A] \left[ S_{\vec{X}'} \right] \Delta \vec{T}_M + c [A] [M] S_{\vec{X}''} \Delta \vec{T}_L \\ &\quad + c [A] [M] [L] \Delta \vec{X}^C - c [A] [M] [L] \Delta \vec{X}^G \\ &= [A] \Delta \vec{x} + [B] \Delta \vec{T}_M + [C] \Delta \vec{T}_L + [D] \Delta \vec{X}^C - [D] \Delta \vec{X}^G \end{aligned} \quad (4-9)$$

4.3 Relationship between Differential Rotation Vector  $\Delta \vec{T}_L$  and Differentials of Rotation Angles ( $\alpha_t, \delta_t, \theta_t$ ):

It is possible to prove the following relations:

$$\Delta \vec{T}_L = \begin{bmatrix} 0 & \sin \alpha & l_{13} \\ 0 & -\cos \alpha & l_{23} \\ 1 & 0 & l_{33} \end{bmatrix} \begin{bmatrix} \Delta \alpha_t \\ \Delta \delta_t \\ \Delta \theta_t \end{bmatrix} \quad (4-10)$$

$$[L] = [l_{ij}] \quad , \quad i = 1,2,3, \quad j = 1,2,3$$

Now assume that only  $\theta_t$  changes with time according to the expression:

$$\theta_t = \theta_0 + \theta_1 t + \theta_2 t^2 \quad (4-11)$$

Then equation (4-10) can be written as:

$$\Delta \vec{T}_L = \begin{bmatrix} 0 & \sin \alpha & l_{13} \\ 0 & -\cos \alpha & l_{23} \\ 1 & 0 & l_{33} \end{bmatrix} \begin{bmatrix} 1 & 0 & 0 & 0 & 0 & 0 \\ 0 & 1 & 0 & 0 & 0 & 0 \\ 0 & 0 & \theta_1 + 2\theta_2 t & 1 & t & t^2 \end{bmatrix} \begin{bmatrix} \Delta \alpha \\ \Delta \delta \\ \Delta t \\ \Delta \theta_0 \\ \Delta \theta_1 \\ \Delta \theta_2 \end{bmatrix} \quad (4-12)$$

Equation (4-12) can be substituted into equation (4-9) resulting in the complete form of the photogrammetric condition equations.

5. Unified Least Squares System (ULSS)

Because of the complexity of the computations involved in the Apollo triangulation, it was necessary to employ a rigorous least squares solution.

ULSS is a software package which allows for automated application of least squares principle in any adjustment program. The advantage of ULSS is that adjustment programs of varying degrees of complexity can be economically constructed. Furthermore, the unification of least squares application into a single software module allows the best guarantee of theoretical and computational integrity of the adjustment operations.

The best way to describe the operations of ULSS is to show its role in a typical adjustment system. Figure 8 is a general functional chart of an adjustment system employing ULSS. The diagram presents ULSS in terms of four major components:

(a) Data Structuring Module:

The function of this module is to change the structure of input data to a special structure which conforms to "Autoray" algorithm for least squares solution. The special data structure is built up into the "Structured Observation" data store within the "Data Base." The data structure produced by this module directly affects the degree of optimization of least squares computations. Data structuring is guided by the parameters which define the adjustment network and by the order in which indirect observations are handled in this program module.

(b) Least Squares Module:

This module operates directly on the "Structured Observation" data store. It adjusts the contents of this data store through the rigorous application of the least squares principle.

In the course of its operation, this module assumes the responsibility of delivering all the needed parameters to the appropriate "Condition Equation Generator" which in turn evaluates condition parameters and hands it back to this module for proper disposition.

(c) Error Propagation Module:

The inversion of the coefficient matrix for the normal equations takes place in this module. The result of the matrix inversion is stored back into the appropriate places within the "Structured Observation" data store.

(d) Data Restructuring Module

This module operations are essentially the reverse of those performed by the Data Structuring Module. The contents of the "Structured Observation" data store are transformed back into a structure similar to that of input data to the Data Structuring Module. The restructured data are placed in the "Unstructured Observations" data store within ULSS Data Base.

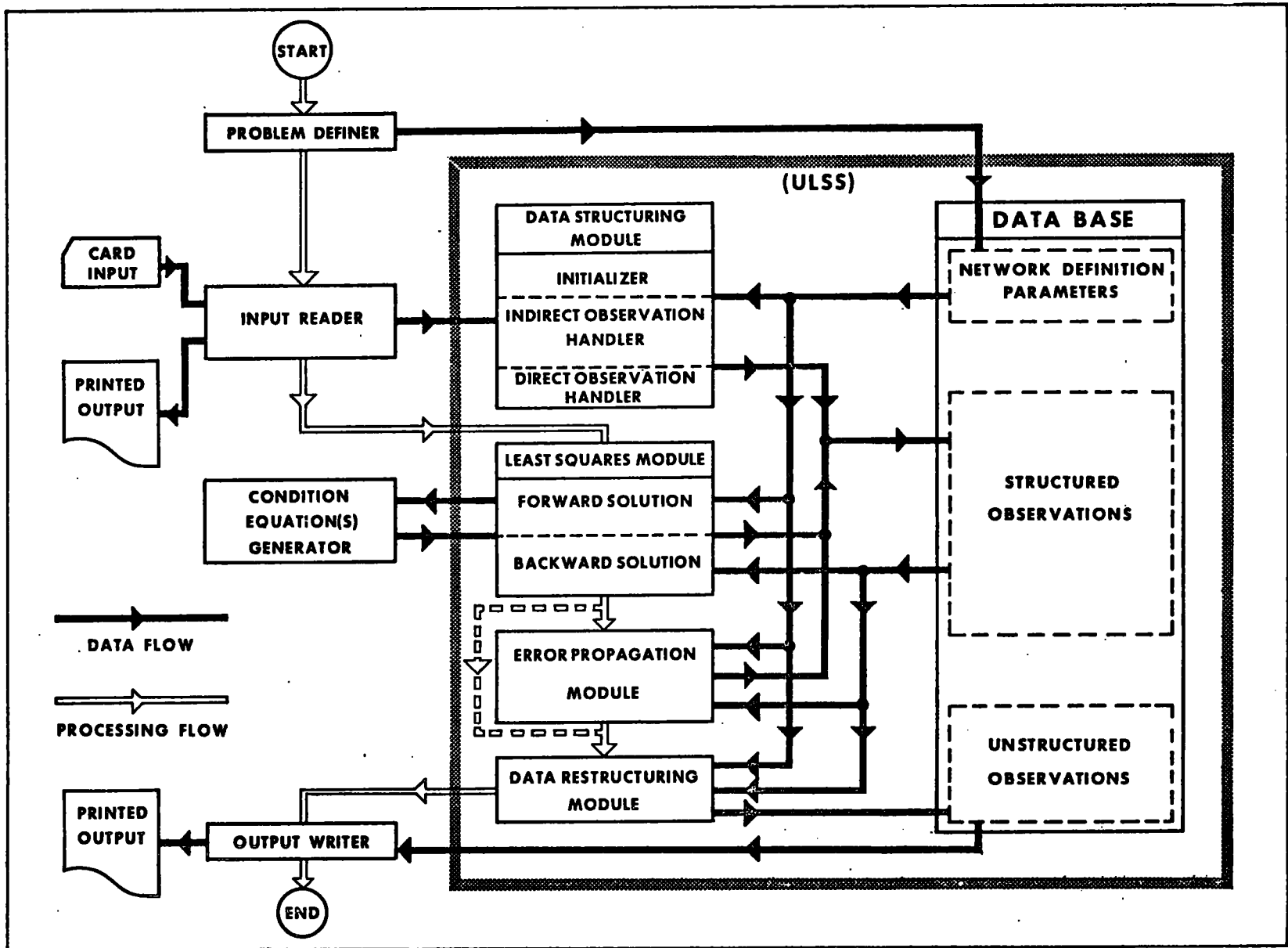


Figure 8.  
Functional Chart of Unified Least Squares System



The capabilities of ULSS are best reflected by the various parameters required for the definition of an adjustment network. ULSS needs object and observation characteristics to guide its operations.

The object under adjustment is characterized by:

(a) Number of object elements (object points, camera parameters, orbit parameters, camera station altitudes, etc.) Ten object elements can be accommodated in the present version of ULSS.

(b) Optimization priorities of object elements. These priorities are needed to guide least squares solution optimization.

(c) Assigned number of characters that identifies members of object elements.

(d) Number of components in the primary parameters of each object element. ULSS presently limits this number to seven. An object element which requires more components may be subdivided into more than one object element.

(e) Number of components in the auxiliary parameters of object elements. The auxiliary parameters are usually direct functions of the corresponding primary parameters.

(f) Maximum number of members in each object element (object points, cameras, orbits, camera stations, etc.)

(g) Logical identification of four data sets for each object element.

(h) Flags identifying each object element as active or non-active in relation to the least squares solution.

(i) Flags identifying the type of covariance matrices for each object element. ULSS will handle full or diagonal covariance matrices.

Observations on the object under adjustment are characterized by:

(a) Number of different types of observations. ULSS in its present form can handle up to ten different types of observations.

(b) Logical identification of Condition Equation Generator for each type of observation.

(c) Number of components for each observation type. The present version of ULSS can accommodate up to four components.

(d) Number of condition equations resulting from each type of observation,

(e) Number and logical identifications of object elements that participate in each type of observation,

(f) Logical identifications of two data sets for each type of observations.

(g) Flags identifying each observation type as active or non-active in relation to least squares solution,

(h) Flags identifying the type of covariance matrices for each observation type. Full and diagonal covariance matrices are allowed in ULSS.

## 6. Photogrammetric Orientation of the Moon

The presence of a terrain camera and stellar camera on the Apollo 15, 16, and 17 missions provided a unique opportunity to perform an independent determination of the orientation of the Moon with respect to the stellar coordinate system. In view of the limited coverage and duration of the three Apollo missions, only a simplified model for the Moon's orientation could be considered. The selected model assumed a fixed orientation for the Moon's rotation axis expressed in terms of the right ascension  $\alpha$  and declination  $\delta$  of the north pole. It also assumes the Moon's rotation rate around its axis to be a linear function of  $t$  and  $t^2$ . The model can be used directly to compute the Moon's orientation parameters or it can be used to compute deviations from any one of the established libration models of the Moon. This second use is of special interest for the following reasons:

- (a) Complicated libration models of the Moon cannot be directly evaluated from the limited photogrammetric data available. However, deviations from these models, which can be assumed to have a simple mathematical form for the duration of the photographic mission can be computed.
- (b) The absence of statistically significant deviations from any of the established Moon libration models is a very strong assurance of the integrity of the data used in the photogrammetric computations of surface coordinates.

The parameterization of the Moon's orientation is described in the mathematical model given in Section 4.

Estimation of the orientation parameters were conducted in a rigorous least squares solution. The task of building the necessary software for the adjustment problem was greatly simplified by the software package entitled "Unified Least Squares Solution (ULSS)," which is described in Section 5. Two separate solutions were computed for the celestial orientation of the axis and rotation rate of the Moon during the Apollo 15 and 16 Missions. Furthermore a separate solution was conducted for the computation of the deviations of the photogrammetric orientation of the Moon from the Eckhardt libration model.

#### 6.1 The Apollo 15 Libration Solution

The data employed in the Apollo 15 solution are given in Table 4. The photographs were selected to give a compact block across the widest part of the total coverage, thus including both first and last photographic passes and encompassing the maximum time span. The results of the solution are shown graphically in figures 9, 10, and 11. The diagrams show the computed values and the 99 percent confidence region derived from the ULSS. Also shown on each diagram is the value of the parameter as given by the Eckhardt libration model.

Table 4  
Data Employed in Apollo 15  
Libration Solution

---

Number of photos.....	44
Number of surface points.....	317
Number of image points.....	1220
Average number of images/surface point.....	3.85
Number of laser altimeter ranges.....	7
Flight duration.....	4 <sup>d</sup> 14 <sup>h</sup> 19 <sup>m</sup>
Moon's angular rotation during mission.....	60° 28' 55"
 Photographic coverage:	
Longitude (70° 03' 27") to (90° 49' 33").....	20° 46' 06"
Latitude (-21° 29' 05") to (8° 08' 41").....	29° 08' 41"
 Mean standard deviation of terrain camera attitude angles	
Roll.....	26".8
Pitch.....	8".8
Yaw.....	23".8
 RMS of image coordinates.....	 9.5μm
Estimated standard deviation of image coordinates.....	12.8μm

---

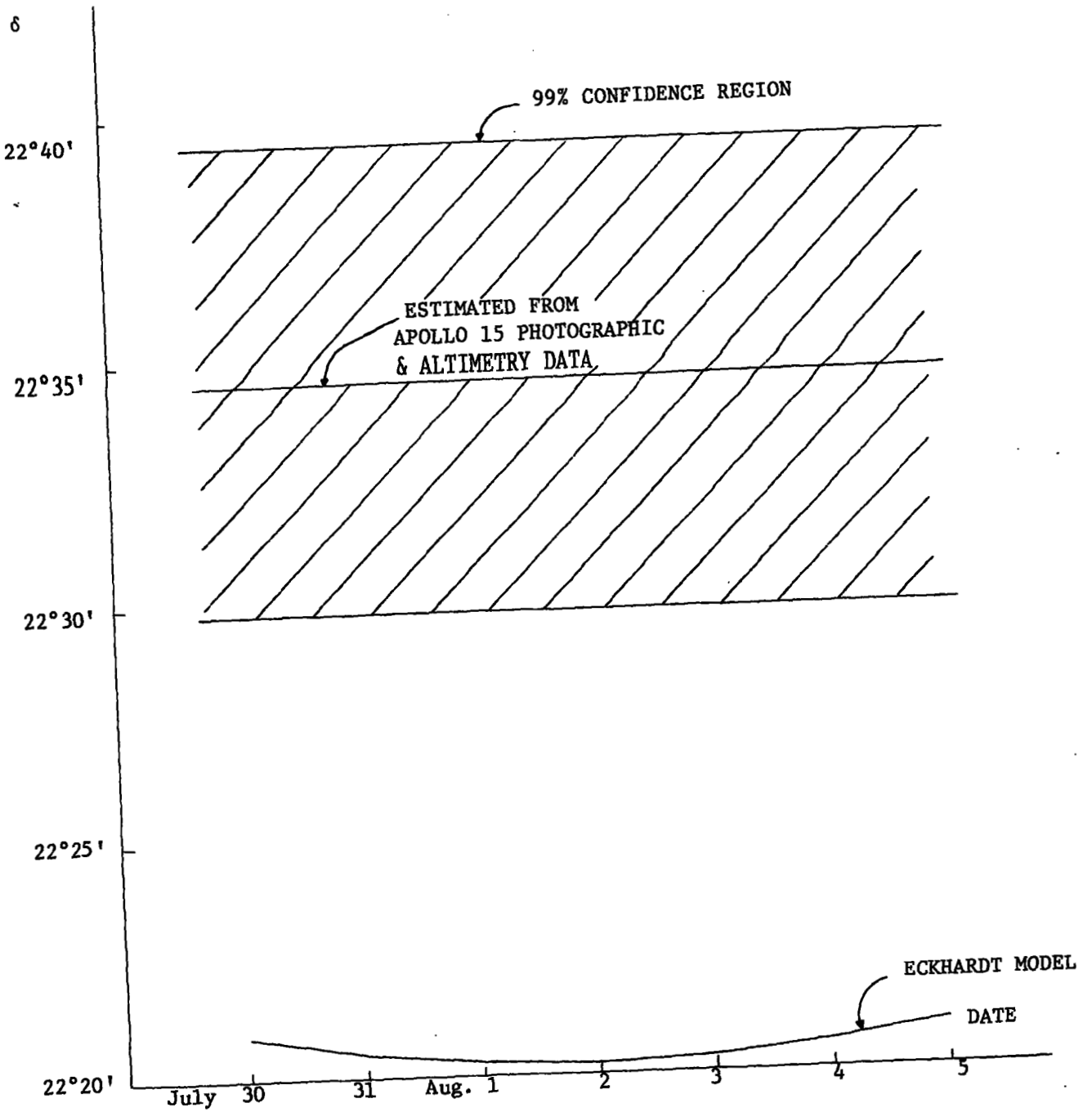


Figure 9.  
 APOLLO 15. North Pole Declination ( $90^\circ - \delta$ ).

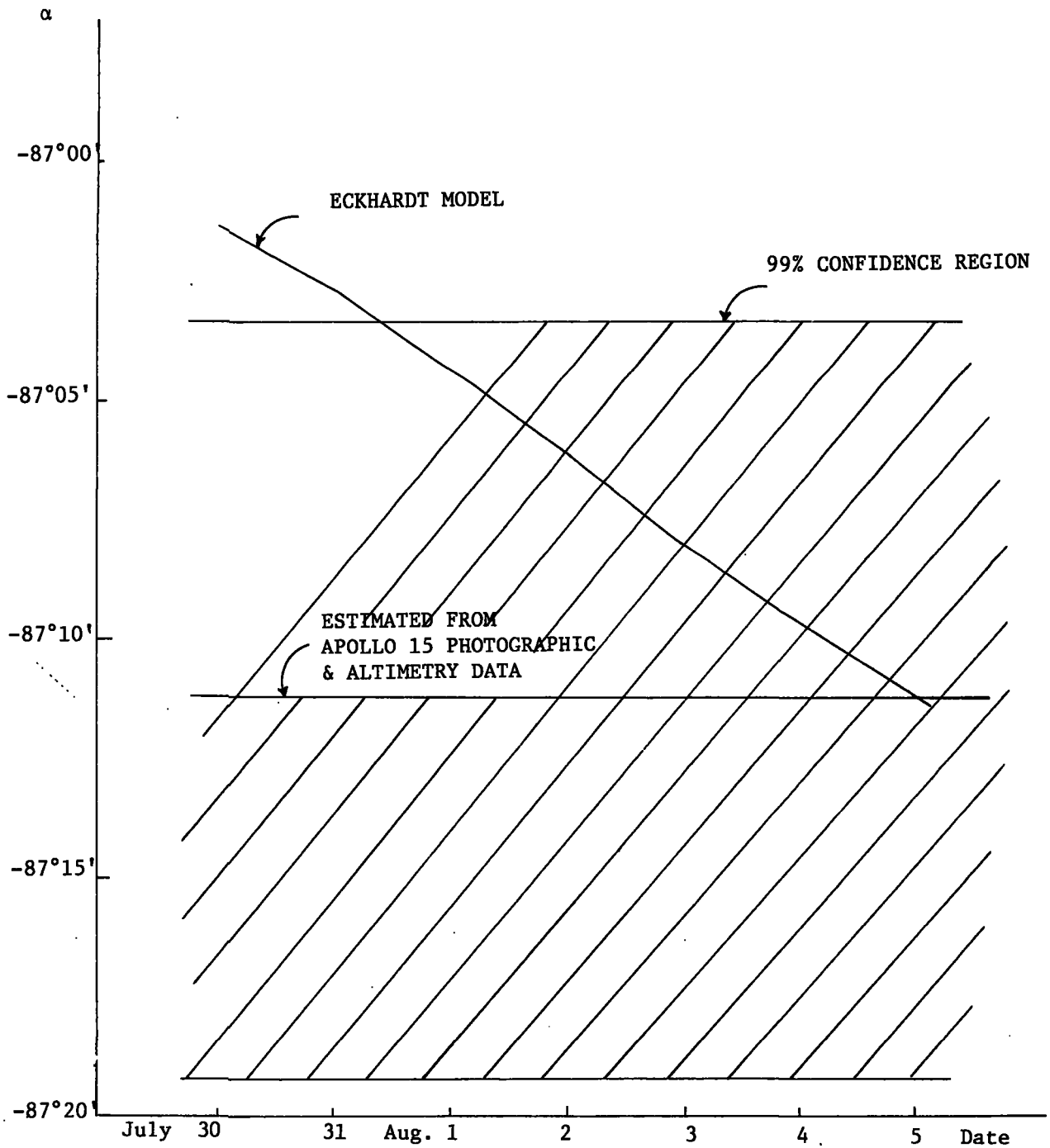


Figure 10.  
 APOLLO 15. North Pole Right Ascension ( $\alpha$ ).

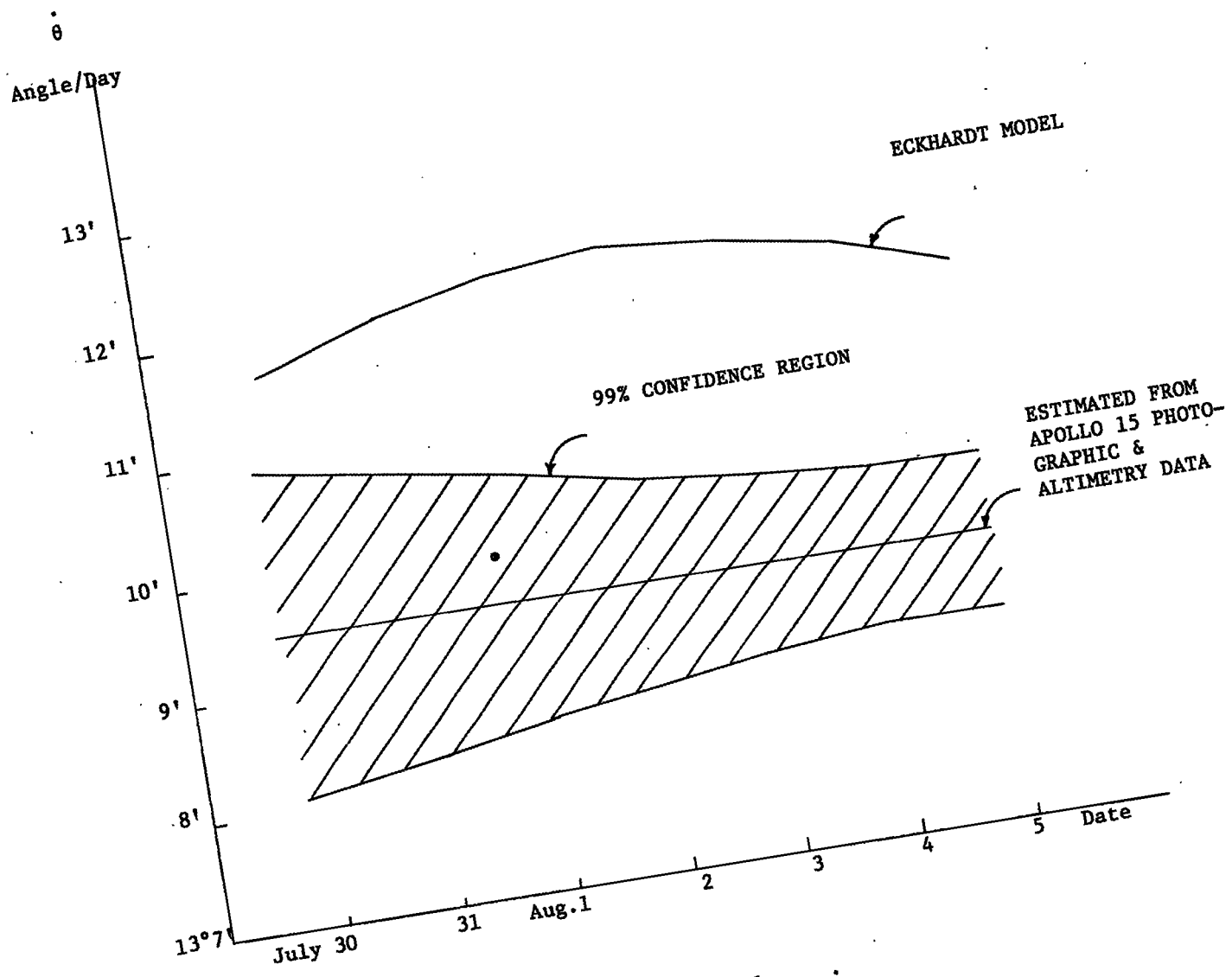


Figure 11.  
 APOLLO 15. Angular Velocity ( $\dot{\theta}$ ).

## 6.2 The Apollo 16 Libration Solution

A similar solution was performed to determine the libration values during the Apollo 16 mission. The data entering this solution are listed in Table 5.

The results of this solution are shown graphically in figures 12, 13, and 14.

## 6.3 Deviations of Moon's Photogrammetric Orientation from Eckhardt Libration Model

In both the Apollo 15 and 16 computed libration solutions, the Eckhardt values fall outside the 99 percent confidence limits for the photogrammetric parameters. This undoubtedly means that the data set was insufficient to determine absolute values of the parameters. For this reason a central photographic block from the three Apollo missions was chosen for the computation of deviations of the Moon's orientation from the latest libration model published by D. H. Eckhardt of Air Force Cambridge Research Laboratories at Hanscom Air Force Base in Massachusetts. A summary of the photogrammetric data is given in Table 6.

The computations involved the evaluation of 13,289 condition equations with the resulting system of normal equations containing 5282 unknowns.

Results of the least squares solution showed deviations between the photogrammetric determination of the Moon's rotation axis and the corresponding values obtained from Eckhardt's libration model to be:

$$\begin{aligned} &= 0'' \pm 12' 56'' \text{ in declination of north pole} \\ \text{and} \\ &= 0'' \pm 12' 55'' \text{ in right ascension of north pole.} \end{aligned}$$

Deviation in the rate of rotation of the Moon were found to be:

$$\begin{aligned} &= 0.529 \cdot 10^{-12} \pm .6027 \cdot 10^{-12} \text{ rad/sec for the } t \text{ coefficient} \\ \text{and} \\ &= 0.833 \cdot 10^{-19} \pm .7582 \cdot 10^{-19} \text{ rad/sec for the } t^2 \text{ coefficient} \end{aligned}$$

These deviations are statistically insignificant and provide positive assurance of the integrity of data used in the analytical triangulation of the Moon's surface points.



Table 5,  
Data Employed in Apollo 16  
Libration Solution

---

Number of photos.....	20
Number of Surface points.....	236
Number of image points.....	918
Average number of images/surface point.....	3.89
Number of laser altimeter ranges.....	15
Flight duration.....	3 <sup>d</sup> 18 <sup>h</sup> 56 <sup>m</sup>
Moon's angular rotation during mission.....	49 <sup>o</sup> 54' 10"
Photographic coverage:	
Longitude (79 <sup>o</sup> 04' 44") to (93 <sup>o</sup> 12' 40").....	14 <sup>o</sup> 07' 56"
Latitude (-6 <sup>o</sup> 08' 35") to (7 <sup>o</sup> 04' 25").....	13 <sup>o</sup> 13' 00"
Mean standard deviation of terrain camera attitude angles	
Roll.....	4".4
Pitch.....	12".9
Yaw.....	3".2
RMS of image coordinates.....	12.9 μm
Estimated standard deviations of image coordinates.....	17.6 μm

---

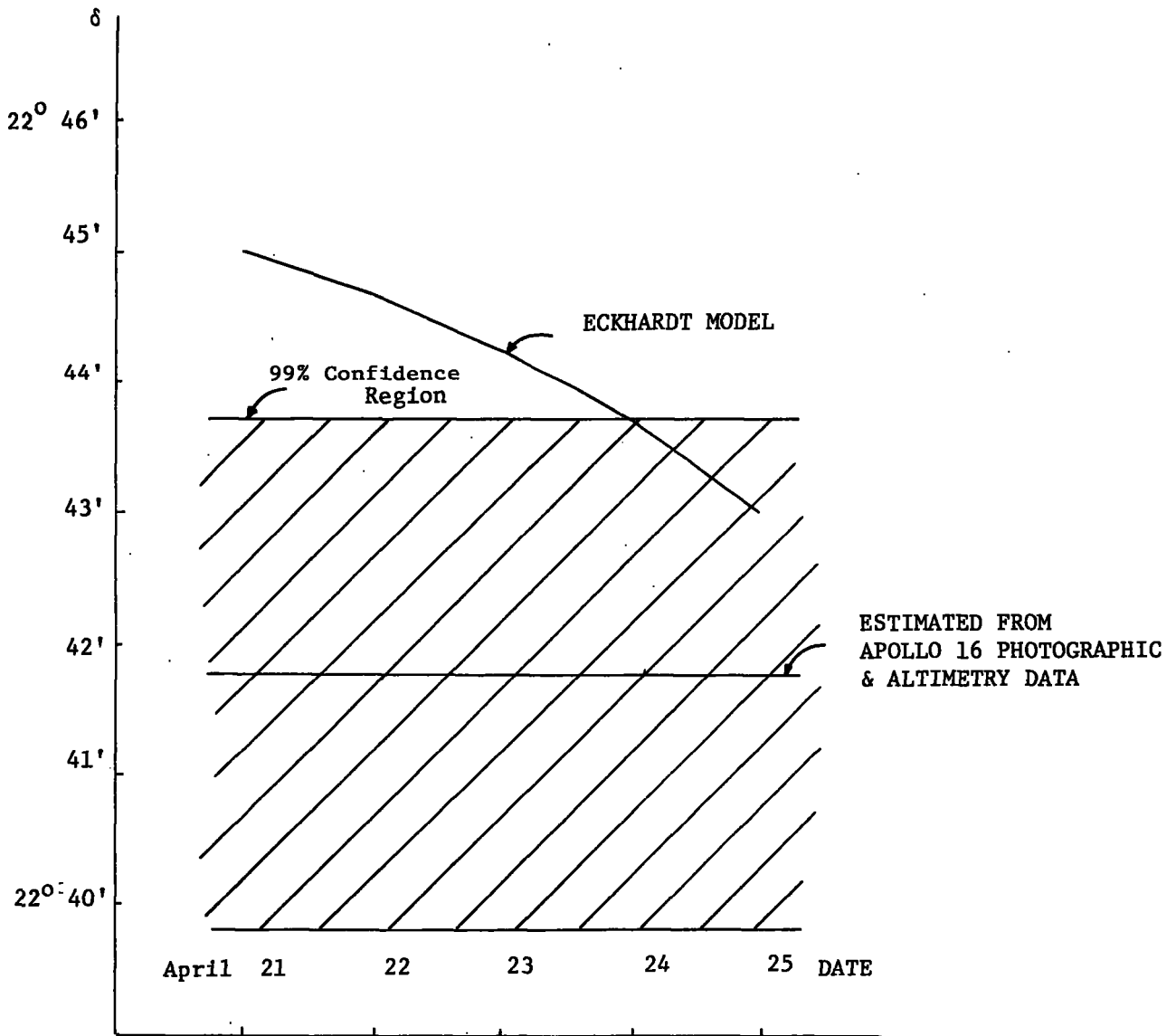


Figure 12.  
 APOLLO 16. Declination of North Pole ( $\delta$ ).

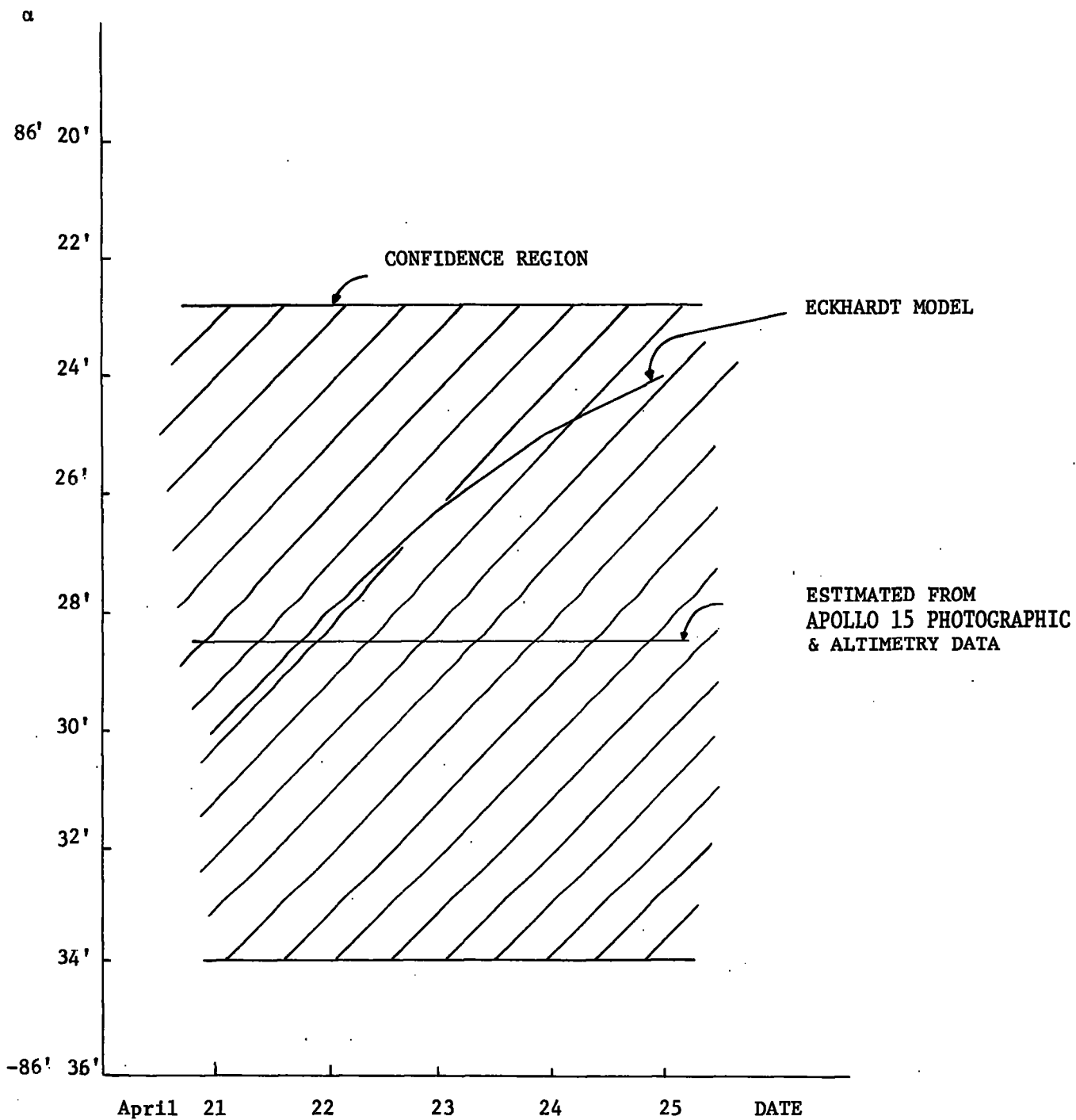


Figure 13.  
APOLLO 16. Right Ascension of North Pole ( $\alpha$ ).

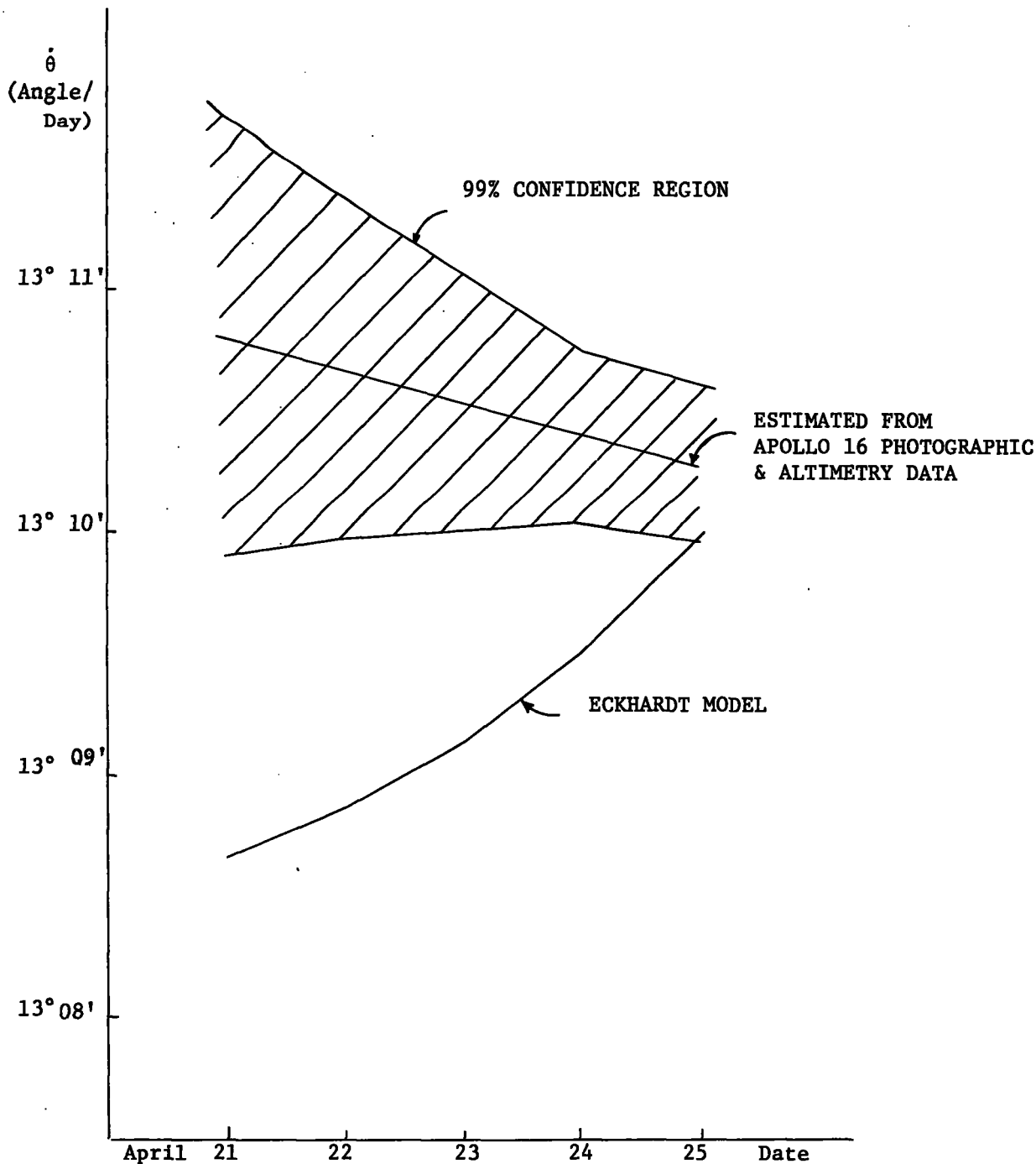


Figure 14.  
 APOLLO 16. Angular Velocity ( $\theta$ ).

Table 6 ·  
Data Employed in Three Mission Libration Solution

---

Number of photos	306
Number of surface points	1044
Number of image points	6575
Average number of images/surface point	6.30
number of laser altimeter ranges	139

Flight duration	(Mission 15)	4 <sup>d</sup> 14 <sup>h</sup> 36 <sup>m</sup> 59 <sup>s</sup>
	(Mission 16)	3 <sup>d</sup> 19 <sup>h</sup> 13 <sup>m</sup> 18 <sup>s</sup>
	(Mission 17)	4 <sup>d</sup> 22 <sup>h</sup> 53 <sup>m</sup> 34 <sup>s</sup>

Photographic coverage:

Longitude (39° 47' 26') to (104° 43' 01") 64° 55' 35"

Latitude (-11° 54' 15") to (13° 11' 23") 25° 05' 38"

A priori estimates of standard deviations for image coordinates

(Mission 15)	9.7 μm
(Mission 16)	19.7 μm
(Mission 17)	7.8 μm

---

## 7. Selenodetic Control Network

The simultaneous solution for 1244 exposure station positions and ground point coordinates for the three Apollo missions 15, 16, and 17 represents the largest single photogrammetric network which has yet been attempted. The normal equations to be solved for 23,000 unknowns would occupy more than half a billion storage locations. To reduce this problem to manageable proportions, some techniques that are in standard use in analytical photogrammetry, and some that are not in general use, were employed.

### 7.1 Bandwidth Minimization

Any large photogrammetric network produces a normal equation matrix which, while it is very large, is also very sparse. Of equal importance, the structure of this matrix is known, and to a large extent can be controlled by the photogrammetrist. By judiciously selecting the order of the unknown parameters, storage of large blocks of zeros can be avoided, thus reducing the computer memory requirement. A standard technique, attributed to D.C. Brown (1958), provides a tremendous saving by eliminating the contribution of all unknown ground points from the matrix that must be retained in core storage. The full normal equation matrix can be partitioned

$$\begin{bmatrix} A & B \\ B^T & C \end{bmatrix}^{-1} = \begin{bmatrix} K & L \\ L^T & M \end{bmatrix} \quad (7-1)$$

where A is quasidiagonal with 6 x 6 submatrices along its diagonal, one for each frame of photography. Likewise, C is quasidiagonal with 3 x 3 submatrices, one for each ground point, along its diagonal. By standard formulas for inversion of partitioned matrices

$$K = (A - BC^{-1}B^T)^{-1} \quad (7-2)$$

and

$$M = C^{-1} + C^{-1}B^TKBC^{-1} \quad (7-3)$$

But since C is quasidiagonal, the unknown ground points can be processed sequentially, without forming either B or C, to obtain a reduced normal equation matrix with the dimensions of A, i.e.,

$$K = (A - \sum_i B_i C_i^{-1} B_i^T)^{-1} \quad (7-4)$$

Once K has been computed, the covariance matrices of the ground points can be computed sequentially from

$$M_i = C_i^{-1} + C_i^{-1} B_i^T K B_i C_i^{-1} \quad (7-5)$$

Of course, application of (7-4) destroys the quasidiagonality of A. A ground point on both the photo represented by the *i*th diagonal block, and the one represented by the *j*th diagonal block will produce an off-diagonal, non-zero block at location *ij*. But since there is a physical limit to the number of photos that can see the same ground points, the reduced normal equations will still be relatively sparse. Judicious ordering of the photos within the original A matrix can keep the nonzero elements close to the diagonal to produce a banded matrix, whose bandwidth is the distance from the diagonal, recorded in 6 x 6 submatrices (or photos), to the farthest off-diagonal nonzero block.

The bandwidth of the reduced normal equations is extremely important because, using a block-bordering algorithm, the matrix inversion process requires that storage be allocated for only *m*(*m*-1) submatrices of dimension 6 x 6. The remainder of the matrix is stored temporarily on disk and read into core, *m* blocks at a time, to replace *m* blocks that have been operated upon and output to disk.

Two attempts were made to minimize the bandwidth of the Apollo photo block using intuition and experience. It is well known that, for regular, parallel strips of photography, minimum bandwidth results from numbering the photos across, rather than along the strips, provided that the number of photos in a strip exceeds the number of strips. Therefore, the first approach was to apply cross-strip numbering to the approximately parallel passes of missions 15 and 17 and to integrate the mission 16 exposures into this numbering scheme in a seemingly logical fashion. This method was used to reorder a 300 photo block from the area of most dense coverage and resulted in a bandwidth of 83 photos requiring a minimum storage of 249,498 locations.

The second method was essentially cross-strip numbering using imaginary strips parallel to the long dimension of the block. The nadir point of each photo was plotted, and a line was constructed through the center of the plot approximately parallel to the long dimension of the block. A template was then slid along this line and the photos were numbered in the order in which their plotted positions were encountered. This method reduced the bandwidth of the 300 photo blocks to 59 photos requiring 126,378 storage locations, but produced an 84 photo bandwidth when applied to the total block.

Finally, it was agreed that intuition was inadequate for this task, and a National Geodetic Survey adaptation of the U.S. Naval Ship Research and Development Center's BANDIT Program was employed. This program utilizes a bandwidth minimization algorithm developed by Cuthill and McKee (1969), and is being used by NGS in the readjustment of the North American Datum. Modifications of this program for use with the Apollo data required several weeks, but proved to be time well spent. The bandwidth of the 300 photo block was reduced to a very tractable 45 photos requiring 73,710 storage locations.

When this program was applied to the total Apollo block, the bandwidth was reduced to 60 photos. This was an extremely fortuitous result, since the maximum bandwidth that could be accommodated by the CDC-6600 computer was 65 photos.

## 7.2 Block Adjustment

Before attempting a simultaneous adjustment, each mission was adjusted individually. This provided: (a) a means for identifying and deleting measurement blunders, (b) a realistic estimate of the image measurement precision for each mission, and (c) better values to be used for initial estimates of the exposure station positions. The individual adjustments were performed on the CDC-6600 computer using the MUSAT IV Program (Elassal et al, 1970). The observed variables consisted of image coordinates, which were assigned a standard deviation of 10 micrometers, and range measurements, assumed to have a standard deviation of one meter. The unknown parameters were the orientation angles of each frame, which were weighted using the covariance matrices obtained from the stellar reductions, and exposure station positions, which were unconstrained.

A large number of measurement and/or identification blunders were detected. Most of these were on Mission 16, which, as mentioned earlier, had not been previously edited. Since the initial density of measured images was so high, especially on Mission 16, deletion of these blunders caused no significant deterioration in the geometric strength of the observations. Therefore, no attempt was made to recover any of these images.

From the individual mission adjustments estimates obtained for the standard deviation of unit weight of an image coordinate were:

Mission 15 -	9.7 $\mu\text{m}$
Mission 16 -	19.7 $\mu\text{m}$
Mission 17 -	7.8 $\mu\text{m}$



These figures indicate that the measurement error on Mission 16 is more than twice that of the other two missions. This is not quite correct. On Mission 16 there are probably a number of "slight misidentifications" which tend to inflate the measurement error. For example a terrain feature may be selected and measured on three consecutive exposures of a single strip with a high degree of precision, but on an adjacent strip a different part of that terrain feature may have been used because of the change in sun angle. The second set of measurements may be equally precise, but a much larger standard deviation will result from combining these two sets of measurements.

DMA-AC recognized this problem in the measurement of Missions 15 and 17. When this situation arose, and if other images in the same area fit across the strips with small standard deviations, they assumed that they had measured a near, but different, terrain point and assigned a new name to it. See, for example, points D6588 and D658H on page A-9 of Appendix A. Since neither point is a significant landmark whose position is of prime importance, there is nothing improper, either mathematically or photogrammetrically, in assuming that what was originally considered to be a single terrain point is actually two very close points. A weak tie between the two strips is sacrificed for a strengthening of the ties between adjacent photos of both strips, and, assuming that a sufficient number of strong ties between the strips exist, the standard deviation of the image measurements has been improved.

In each individual mission adjustment the exposure station positions obtained from the tracking orbits were used as initial estimates, but were permitted unconstrained adjustment. However, the position of one exposure station on each mission was held fixed and served as the only positional constraint. Therefore each mission was initially adjusted to its own arbitrary origin of coordinates. Eventually one terrain point, 22051, was chosen to be the only positional constraint for the simultaneous adjustment. This point is near the center of the block, appears on at least three exposures in every mission, and obtained small image measurement residuals in all individual mission adjustments. The mean of the three positions obtained for terrain point 22051 from the individual adjustments was assigned to this single control point.

In the simultaneous adjustment, as in the individual adjustments, the laser range data were treated as observed variables with a standard deviation of one meter, and they provided the necessary scale constraint. The image coordinates completed the set of observables and were assigned the standard deviation of unit weight for the mission to which they belonged as derived from the individual adjustments.

A total of 51,138 image coordinates and 519 altimeter observations were used in the solution.

There were three types of parameters computed in the adjustment. The three orientation angles of each frame were parameterized, but assigned, a priori, the covariance matrices obtained from the stellar reductions. This set of constrained parameters furnished the orientation of the block. The remaining parameters, the positions of all exposure stations and the positions of all terrain points (except 22051), were completely unconstrained. No orbital constraints of any kind were employed; the position of the entire block was established by the single control point 22051. In all, 23,436 parameters were determined: three position and three orientation components for each of 1,244 photographs and three coordinates of each of 5,324 terrain points.

As in the individual adjustments the MUSAT IV Program was employed. Five iterations were required; three for the first edit cycle and one for each of two additional edit cycles. The simultaneous adjustment required the entire memory of NOAA's CDC-6600 computer (330,000 octal words) and took 14 hours of clock time (4 hours and 40 minutes of central processor time). Every three hours the processing was interrupted and the total computer environment, including the contents of all disk files, was recorded on magnetic tape in order to provide a restart capability in the event of a malfunction of any type. This proved to be unnecessary due to the diligence and cooperation of the computer operations staff, and the total adjustment was completed on the first try.

Since the position of the block was determined by an assumed position of one terrain point, the computed positions of all exposure stations and terrain points are consistent with one another, but are referred to an arbitrary origin of coordinates. DMA used the tracking ephemeris of revolution 44 of Mission 15 as position constraints and, thereby, referred their mapping to the center of mass of the Moon as defined by that orbit. In order to minimize the discrepancies between the NOS/GS computed positions and the DMA results, the same coordinate origin was chosen. After the adjustment had been completed all positions were translated, but not rotated, to best fit the tracking ephemeris of revolution 44 of Mission 15.

### 7.3. Results of Block Adjustment

A summary of the results of covariance propagation to the computed terrain point positions is shown in figure 15. The standard deviations

in horizontal position, shown in this figure, are radii of probability circles, i.e.,

$$\sigma_H = R(\sigma_\phi^2 + \sigma_\lambda^2 \cos^2 \phi)^{1/2}$$

where R is the mean radius of the Moon, and the variances in latitude and longitude ( $\sigma_\phi^2, \sigma_\lambda^2$ ) are in (radians)<sup>2</sup>. There was little difference between the standard deviations in horizontal position,  $\sigma_H$ , and elevation,  $\sigma_E$ . for the individual ground points represented by these bar graphs. For 70% of the points,  $\sigma_H$  is less than 30 meters, and for 74%,  $\sigma_E$  is less than 30 meters, a result that is quite respectable in comparison with previous lunar control networks.

Slightly more than one percent of the points have standard deviations greater than 100 meters and a few exceed 1,500 meters. The reason for the lack of precision in the positions of these points becomes obvious with reference to figure 16, which shows the spatial distributions of the standard deviations,  $\sigma_H$  and  $\sigma_E$ . The shaded areas, inside the  $\sigma = 30$  meters contours, are essentially the same on both maps and coincide with the area of most dense photo coverage and laser ranging. Inside these areas, there are a few points at which  $\sigma > 30$  meters (see Appendix A), which are the result of a terrain point having been observed on only two or three photographs. Near the ends of the strips, all points are observed on no more than three photographs, and there is a substantial increase in the standard deviations as seen on the left-hand edge of the maps. On the left-hand edge, and particularly the lower left, the absence of adjacent passes combined with the complete lack of range observations causes a very substantial increase in  $\sigma_E$  and a tremendous increase in  $\sigma_H$ . Obviously, the photogrammetry was incapable of extrapolating over large distances without benefit of scale control, but initially it seems strange that horizontal position errors should increase more rapidly than elevation errors.

The photographs in this area are all from mission 16. Strip G of that mission terminates at a point near the 120 meter contour line for horizontal position. The area to the east of this point is covered by both strips G and R, with a range observation controlling the scale of each frame of strip G. West from this point, there is only strip R and no range observations; a situation similar to the classical cantilever extension, except that the attitude orientation of each frame is well determined from the stellar data.

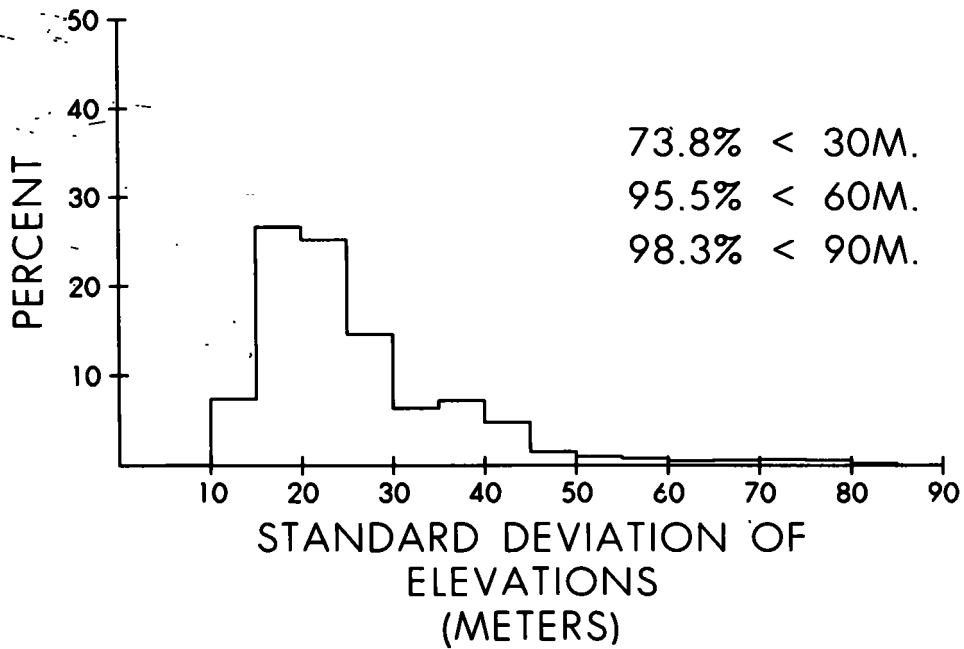
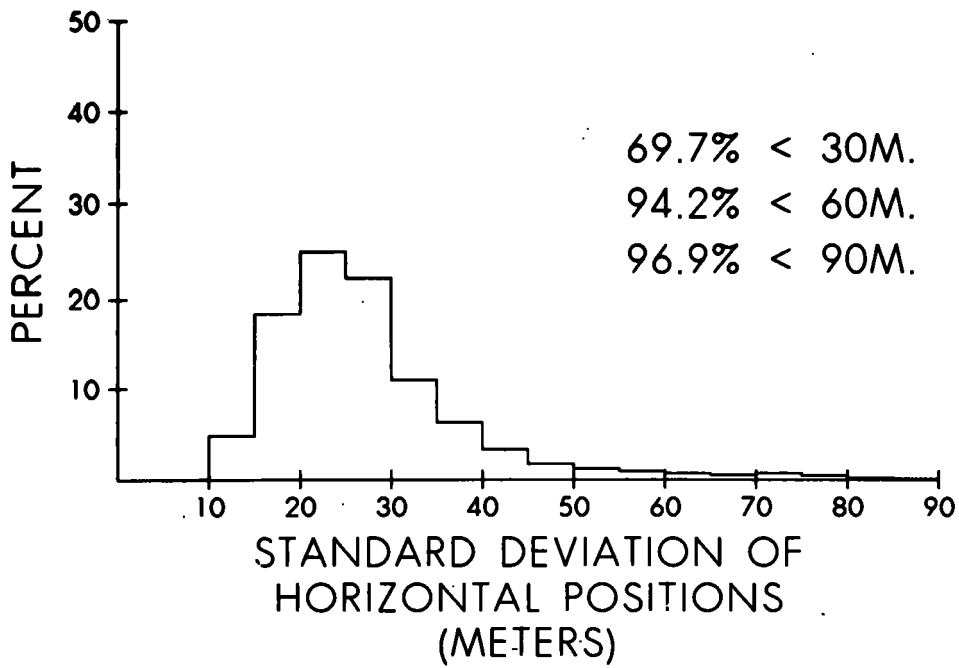
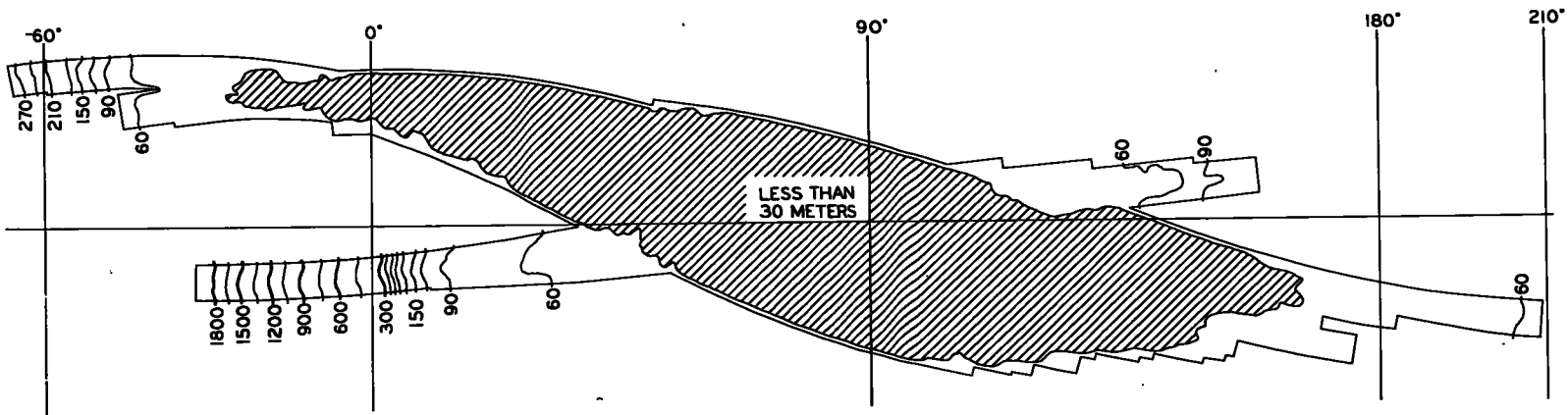


Figure 15.  
Standard deviation of terrain positions.



STANDARD DEVIATION OF HORIZONTAL POSITIONS

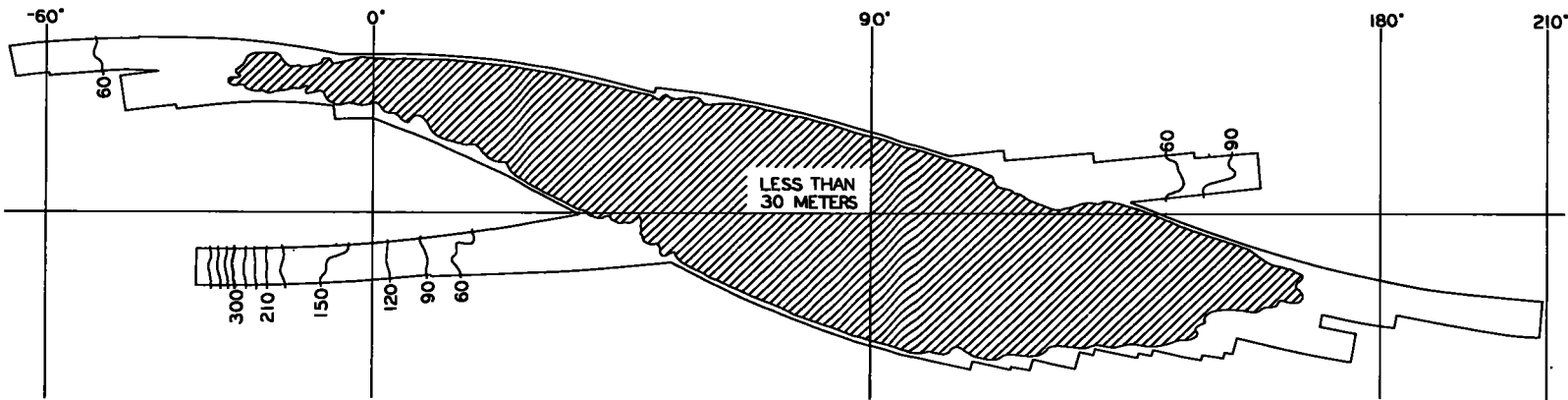


Figure 16.  
Spatial Distribution of Standard Deviations.

Since the uncertainties in the terrain point positions are directly related to uncertainties in the positions of exposure stations from which they are intersected, it is informative to consider the standard deviation in the exposure station positions. From Table 7, in which the standard deviation in horizontal positions of the exposure stations are separated into components of Northing and Easting, it is apparent that the increase in  $\sigma_H$  is almost entirely the result of uncertainties in Easting, which is the along-track coordinate.

Table 7.  
Components of Standard Deviation for  
Selected Exposure Stations.

Frame No.	Standard Deviation in			Frame No.	Standard Deviation in		
	Northing	Easting	Elevation		Northing	Easting	Elevation
G66	28	64	48	R48	29	64	49
G67	29	67	49	R49	30	68	51
G68	30	71	51	R50	31	74	54
				R51	31	95	60
				R52	33	136	67
				R53	38	201	76
				R54	42	282	88
				R55	47	378	103
				R56	51	485	122
				R57	56	601	147
				R58	59	727	177
				R59	60	862	213
				R60	61	1006	256
				R61	59	1156	305
				R62	57	1311	362
				R63	55	1471	427
				R64	55	1636	499
				R65	59	1804	578

The along-track coordinate is almost entirely dependent upon scale transfer between stereomodels. It is well known that scale transfer dependent upon image points only increases as the square of the number

of models. Prevention of this scale error propagation was the fundamental reason for including the laser altimeter observations as a scale restraint. The lack of altimeter data in the western limits of Apollo 16 is undoubtedly the major reason for the along-track uncertainties.

As mentioned above, strip R, frames R50 through R65, approximates a cantilever extension in which the uncertainties in elevation would normally be expected to increase at a greater rate than those of the other two coordinates. Since the results shown in Table 7, in which the along-strip uncertainties increase much faster than the elevation uncertainties, are contrary to those obtained from classical cantilever extension, it appears that the attitude constraints are reducing the rate of increase in elevation errors. In order to verify this theory, a computer simulation was performed. A strip of five photographs was devised with the usual nine pass points per photo. There were three control points, all in the first model, and the attitudes of all photos were weighted so heavily as to remove them from the adjustment. The results of this simulation are given in Table 8.

Table 8.  
Components of Standard Deviation  
for Simulated Test.

Photo No.	Standard Deviation		
	Along Strip	Across Strip	Elevation
1	0.77	0.56	1.00
2	1.48	0.70	1.50
3	3.59	0.83	1.65
4	6.27	0.94	1.86
5	9.43	1.05	2.04

They show that, under the assumption of precisely determined attitude parameters from an external source, the along-strip errors in a cantilever extension do indeed increase at a greater rate than the elevation errors. Hence the large standard deviations that appear in figure 16 near the ends of the strips are a logical consequence of the distribution of photo coverage and laser range observations.

Since there is such a large area of the block in which the standard deviations are less than 30 meters, and since all strips pass through this area, the results of this photogrammetric adjustment may provide a means for improving the post-flight orbit analysis. If reliable orbits could be determined, using this approach, the uncertainties in terrain point positions near the ends of the strips could be vastly improved.

The computed positions of all terrain points are given in Appendix A where they are organized according to accepted lunar map sheets. Exposure station positions are given in Appendix B where they are organized according to Mission and photographic Rev number. Appendices A and B are published separately.

## 8. Conclusions and Recommendations

The work performed on this contract led to several significant conclusions and recommendations.

### 8.1 Conclusions

(a) The total mapping camera coverage produced by Apollo missions 15, 16, and 17 was disappointing in extent. Most damaging was the failure to complete an arc completely around the Moon. This would have permitted the block triangulation to close upon itself rather than hanging loose at the end of each mission. As a consequence, standard errors of position and elevation would probably have been around 30 meters throughout the block, rather than building up to several hundred meters at the ends of the unconstrained strips as shown in figure 16.

(b) The integrity of the photogrammetric solution greatly exceeded that of the orbital tracking data. Consequently the single simultaneous solution performed by NOS/USGS may be expected to be more homogeneous in accuracy and precision than the DMA solution in which orbital constraints were employed.

(c) The Eckhardt libration model used in the NOS/USGS solution has appreciable advantages over the more primitive Koziel model used in the DMA solution. The choice of the Eckhardt model results in significant differences in the selenocentric coordinate systems in the two solutions (see page 18). Although the NOS/USGS solution was eventually adjusted to the Apollo 15 rev 44 tracking data used as basic control by DMA, this adjustment was a translation only and not a rotation. The consequence is that both solutions have their coordinate origin at the same center of mass, but the superior angular orientation provided by the Eckhardt libration model is preserved in the NOS/USGS solution.



(d) The Apollo stellar data sets were inadequate to provide a valid independent solution for libration parameters (see figures 9 through 14) but the correctness of the theory derived in Section 4 is demonstrated by the statistically insignificant computed differences between the Apollo solution and the Eckhardt model as described in Section 6.3. This computation also demonstrated that there is no inconsistency between the Apollo data and the Eckhardt libration model. A similar comparison between the Apollo data and the Koziel model could have been performed, but it would certainly have shown the difference in angular orientation described on page 18.

(e) The exposure station positions and ground point coordinates computed in the NOS/USGS solution represent the most accurate and homogeneous set of values obtainable from the Apollo photogrammetric data. Any further refinement would be dependent upon:

- o Improved and homogeneous positions for camera exposure stations resulting from recomputation of orbital ephemerides. These would be particularly valuable at the limits of the coverage where the photogrammetric error propagation shows large standard deviations (see figure 16).

or

- o A grand simultaneous solution involving photogrammetric condition equations, gravity model parameters, unknown spacecraft thrusting, libration parameters, and spacecraft tracking data. However it is doubtful if the limited extent of Apollo data warrants such a solution.

(f) Although one of the original objectives of the research was to compute a new lunar ellipsoid, the failure to close the equator and the large standard deviations in coordinate positions at the ends of the unconstrained strips made it evident that this would not be a useful thing to do.

## 8.2 Recommendations

(a) The most obvious recommendation is that the photographic task should be completed. One of the greatest scientific disappointments of the Apollo Program was the failure to accomplish complete photographic coverage with the metric camera. There is now no NASA plan which will rectify this shortcoming. But it will be done sometime in the future -- if not by NASA, perhaps by the USSR.

(b) The exposure station positions given in Appendix B should be used in any further attempt to refine the orbits of Apollo missions 15, 16, and 17. It is important to recognize the systematic differences between these positions and those provided by the DMA solution. These systematic differences result from the use by

NOS/USGS of the improved Eckhardt libration model while the DMA solution employed the earlier Koziel model. Thus the NOS/USGS solution coincides better with the real geometric situation of the Moon.

If the exposure station values are used in any further attempts to improve mission ephemerides, only those having standard deviations of 30 m or less should be included, unless a sophisticated weighting scheme is employed based upon the listed standard deviations

(c) It is unfortunate - though perhaps inevitable - that the current lunar mapping program is based upon control established by the DMA solution. The systematic differences between the two solutions (up to 640 m in latitude and 1938 m in longitude, see page 18) result in sensible displacements of the map graticule even at the smallest scale as shown in Table 9.

Table 9 .  
Systematic Differences in Map Graticule  
Resulting from Choice of Libration Model .

Map scale	$\Delta\phi = 640\text{m}$	$\Delta\lambda = 1938\text{m}$
1: 50,000	12.80 mm	38.76 mm
1: 250,000	2.56 mm	7.75 mm
1:1,000,000	0.64 mm	1.94 mm
1:5,000,000	0.13 mm	0.39 mm

Though there is undoubted merit in consistency of reference system between map series, the change to the better system ought to be made sometime. Perhaps it could be done for the new 1:1,000,000 sheets in the Apollo data area for which production is just beginning. It should also be done for the 1:5,000,000 map, although this would mean recomputation of all other control outside the Apollo area.

(d) Of fundamental importance is the identification of the lunar surface features whose positions have been determined by this (and the DMA) solutions. The coordinates of these features are of no use to anyone without the feature identification. These identifications exist only as marked on the photographs employed for mensuration by DMA. A set of prints, films, microfilms - or any other acceptable means - on which the selected points can be clearly seen should be deposited in the National Space Science Data Center for use by future investigators.

(e) Many more surface points were measured by DMA than were used in the NOS/USGS triangulation solution. The positions of these points can be easily determined by intersection computations using the already available exposure station positions and camera attitudes. If it is elected to use the NOS/USGS control system for any future mapping, the positions of these additional points should be determined.

## References

- Brown, D. C., A solution to the general problem of multiple station analytical stereotriangulation, RCA Data Reduction Technical Rpt. No. 43, February 1958.
- Cuthill, E., and McKee, J., Reducing the bandwidth of sparse symmetric matrices. Proceedings of Association for Computing Machinery, 24th National Conference, August 226-28, 157-172.
- Eckhardt, D.H., Physical librations due to the third and fourth degree harmonics of the lunar gravity potential, Moon, 6, 127-134, 1973.
- Elassal, A.A., Brewer, R.K., Gracie, G., and Crombie, M., MUSAT IV, Final Technical Rpt., Raytheon Company, Alexandria, Va., 1970.
- Kaula, W. M., The gravity and shape of the Moon, EOS, Transactions American Geophysical Union, 56, 309-316, 1975.
- Williams, J.G., Slade, M.A., Eckhardt, D.H.. and Kaula, W.M., Lunar physical librations and laser ranging, Moon, 8, 469-483. 1973.



NOAA Technical Reports National Ocean Survey,  
National Geodetic Survey Subseries

- NOS 65 NGS 1 The Statistics of residuals and the detection of outliers. Allen J. Pope, May 1976, 133 pp.
- NOS 66 NGS 2 Effect of Geociever observations upon the classical triangulation network. Robert E. Moose and Soren W. Henriksen, June 1976, 65 pp.
- NOS 67 NGS 3 Algorithms for computing the geopotential using a simple-layer density model. Foster Morrison, in press.
- NOS 68 NGS 4 Test results of first-order class III leveling. Charles T. Whalen and Emery Balazs, November 1976, 30 pp.

NOAA Technical Memorandums National Ocean Survey,  
National Geodetic Survey Subseries

- NOS NGS 1 Use of climatological and meteorological data in the planning and execution of National Geodetic Survey field operations. Robert J. Leffler, December 1975, 30 pp.
- NOS NGS-2 Final report on responses to geodetic data questionnaire. John F. Spencer, Jr., March 1976, 39 pp.
- NOS NGS-3 Adjustment of geodetic field data using a sequential method. Marvin C. Whiting and Allen J. Pope, March 1976, 11 pp.
- NOS NGS-4 Reducing the profile of sparse symmetric matrices. Richard A. Snay, June 1976, 24 pp.
- NOS NGS-5 National Geodetic Survey data: Availability, explanation, and application. Joseph F. Dracup, June 1976, 39 pp.
- NOS NGS-6 Determination of North American Datum 1983 coordinates of map corners. T. Vincenty, October 1976, 8 pp.

## NOAA SCIENTIFIC AND TECHNICAL PUBLICATIONS

NOAA, the *National Oceanic and Atmospheric Administration*, was established as part of the Department of Commerce on October 3, 1970. The mission responsibilities of NOAA are to monitor and predict the state of the solid Earth, the oceans and their living resources, the atmosphere, and the space environment of the Earth, and to assess the socioeconomic impact of natural and technological changes in the environment.

The six Major Line Components of NOAA regularly produce various types of scientific and technical information in the following kinds of publications:

**PROFESSIONAL PAPERS** — Important definitive research results, major techniques, and special investigations.

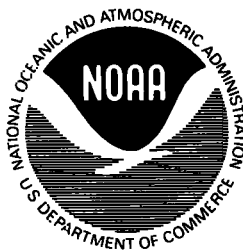
**TECHNICAL REPORTS**—Journal quality with extensive details, mathematical developments, or data listings.

**TECHNICAL MEMORANDUMS** — Reports of preliminary, partial, or negative research or technology results, interim instructions, and the like.

**CONTRACT AND GRANT REPORTS**—Reports prepared by contractors or grantees under NOAA sponsorship.

**TECHNICAL SERVICE PUBLICATIONS**—These are publications containing data, observations, instructions, etc. A partial listing: Data serials; Prediction and outlook periodicals; Technical manuals, training papers, planning reports, and information serials; and Miscellaneous technical publications.

**ATLAS**—Analysed data generally presented in the form of maps showing distribution of rainfall, chemical and physical conditions of oceans and atmosphere, distribution of fishes and marine mammals, ionospheric conditions, etc.



*Information on availability of NOAA publications can be obtained from:*

**ENVIRONMENTAL SCIENCE INFORMATION CENTER  
ENVIRONMENTAL DATA SERVICE  
NATIONAL OCEANIC AND ATMOSPHERIC ADMINISTRATION  
U.S. DEPARTMENT OF COMMERCE**

**3300 Whitehaven Street, N.W.  
Washington, D.C. 20235**